Computer Modeling in
Engineering & Sciences

Tech Science Press

https://doi.org/10.32604/cmes.2026.079665

ARTICLE

# Assessment of Regional Structural Optimality in a 2D Synthetic Proximal Femur Model under Varying Loading Angles

**Jisun Kim and Jung Jin Kim***

Department of Mechanical Engineering, Keimyung University, Daegu, Republic of Korea

*Corresponding Author: Jung Jin Kim. Email: kjj4537@gmail.com

Received: 26 January 2026; Accepted: 23 March 2026; Published: 27 May 2026

**ABSTRACT:** Synthetic proximal femur models avoid the ethical and technical limitations of human specimens and thus serve as an effective alternative for studying the proximal femur. This structure is directly connected to the hip joint, endures complex multi-directional loads, and exhibits region-specific structural adaptations due to its unique triangular geometry. However, most previous studies have examined only global load distributions or restricted regions, limiting the understanding of regional structural optimality. Therefore, this study aims to quantitatively evaluate the load adaptability and structural optimality of the proximal femur across individual regions of interest (ROIs). Three types of 2D finite element models of synthetic proximal femur models are generated. Structural analyses are then performed by varying the loading angles of hip contact and muscle forces. Finally, the proximal femurs are divided into different sizes of grids, and the load adaptability of different ROIs was to evaluated regional structural optimality. The proximal femur exhibited region-specific differences in structural optimality and load adaptability under varying loading angles. The femoral head and greater trochanter exhibited high conformity, while the femoral neck showed consistently low conformity, demonstrating that local anatomical features play a decisive role in load adaptability. Lower model resolution reduced predictive accuracy, whereas increasing ROI size improved stability by reducing local variability. This study establishes a quantitative framework for assessing regional structural optimality in synthetic proximal femurs. The findings demonstrate anatomy-dependent load adaptability and provide foundational insight for future 3D modeling and clinical translation.

**KEYWORDS:** Synthetic proximal femur models; structural optimality; load adaptability; finite element analysis; conformity index; loading angles

## 1 Introduction

Synthetic proximal femur models have been widely employed as reliable surrogates to replicate the complex geometry and mechanical behavior of the human proximal femur. By closely replicating the anatomical morphology and mechanical properties of the femur, these models ensure repeatability and reliability in quantitative experiments and numerical analyses [1–3]. Moreover, they overcome the ethical and technical limitations associated with the use of actual human bone specimens and have served as surrogate models in biomechanical research to investigate the mechanical response of the proximal femur. Importantly, because the loads applied to the femur are difficult to predict, synthetic proximal femur models provide insights into the given loading conditions and the resulting bone structures, enabling the analysis of the relationship between the applied loads and bone morphology [4–7].

Copyright © 2026 The Authors. Published by Tech Science Press. This work is licensed under a Creative Commons Attribution 4.0 International License, which permits unrestricted use, distribution, and reproduction in any medium, provided the original work is properly cited.

The human skeletal system adapts to externally applied mechanical loads by altering the bone structure and density, ultimately forming an optimized structural configuration [8–11]. Among the bones in the human body, the femur most clearly demonstrates such adaptability as it is the largest structure supporting the body weight and is responsible for effectively distributing the complex loads generated during daily activities [12–14]. This adaptive process is well explained by Wolff's law [15], which states that bones remodel themselves under the action of repetitive mechanical stimuli to maintain structural stability. Understanding this adaptability is essential for investigating femoral biomechanics, and such processes can be virtually simulated using synthetic proximal femur models [16].

The proximal femur is directly connected to the hip joint and is continuously exposed to loads of varying directions and magnitudes [17–19]. This complex loading environment imposes diverse mechanical stimuli across the entire femur, and when combined with its intrinsic anatomical and structural characteristics, leads to region-specific differences in load adaptability [12,20,21]. These differences are fundamentally associated with the characteristic triangular structural geometry of the proximal femur, in which the superior, medial, and lateral cortical walls converge in the coronal plane to form a high-modulus framework [22,23]. This triangular configuration not only enhances the overall femoral stability by reducing bending moments, balancing shear forces, and improving load transfer efficiency but also serves as a key factor in inducing distinct patterns of load adaptability across different regions. However, attempts to quantitatively evaluate such region-specific adaptations and structural optimality remain limited because most existing studies have primarily focused on the global load distribution or localized stress concentrations. In fact, many prior studies have assessed the load adaptability of the proximal femur only at the whole-structure level or restricted their analyses to limited regions such as the femoral head and neck. Such approaches are insufficient to systematically reveal the differences in load adaptability across regions [24–28]. Therefore, a precise quantitative evaluation at the region-of-interest (ROI) level is required to better understand the region-specific structural adaptations of the proximal femur.

An ROI-level evaluation becomes particularly important considering that the structural responses of the femur may vary depending on the loading conditions derived from daily activities. In fact, only a few studies have systematically analyzed the differences in the load distribution or quantitative variations at the ROI level under representative loading scenarios such as one-legged stance, adduction, and abduction. Moreover, there is a need to clarify the structural adaptability of the proximal femur to loading under complex conditions in which the hip contact forces (HCFs) and muscle forces (MFs) of different origins act simultaneously [29]. Existing studies have often relied on simplified load models based on the foundational work by Beaupré et al. or have averaged the loads under specific motions; however, these approaches have not been extended to region-specific adaptability assessments [27,30–33]. Therefore, a more precise analysis of the load adaptability of the proximal femur would require a new approach that incorporates a regional-level quantitative assessment and diverse loading conditions.

This study aimed to quantitatively evaluate the load adaptability and structural optimality of the proximal femur across individual ROIs using synthetic proximal femur models. To this end, three synthetic proximal femur models were generated under representative loading scenarios: one-legged stance, adduction, and abduction. Variations in the stress distribution and strain energy density (SED) were analyzed by altering the applied angles of the HCFs and MFs. Moreover, the effects of model resolution and ROI size on the predictive accuracy of structural optimality were examined, enabling quantitative comparisons of the structural adaptability of the proximal femur under different model resolutions, ROI sizes, and loading conditions. Through a regional conformity analysis, this study aimed to elucidate the functional structural adaptability of the proximal femur and provide quantitative data and evaluation indices that may contribute to customized implant and scaffold designs, fracture prevention, and rehabilitation strategies.

## 2 Methodology

The load adaptability and region-specific structural optimality of the proximal femur were investigated by quantitatively analyzing the load dependency of each ROI under various external loading conditions and identifying the dominant load condition through a systematic three-step methodology, as outlined in Fig. 1. First, a synthetic proximal femur model was generated for the load adaptability analysis (Section 2.1). Second, a finite element (FE) structural analysis was performed by varying the loading angles of HCFs and MFs (Section 2.2). Finally, the proximal femur was divided into grids, and the load adaptability of different ROIs was quantitatively assessed to evaluate regional structural optimality (Section 2.3).

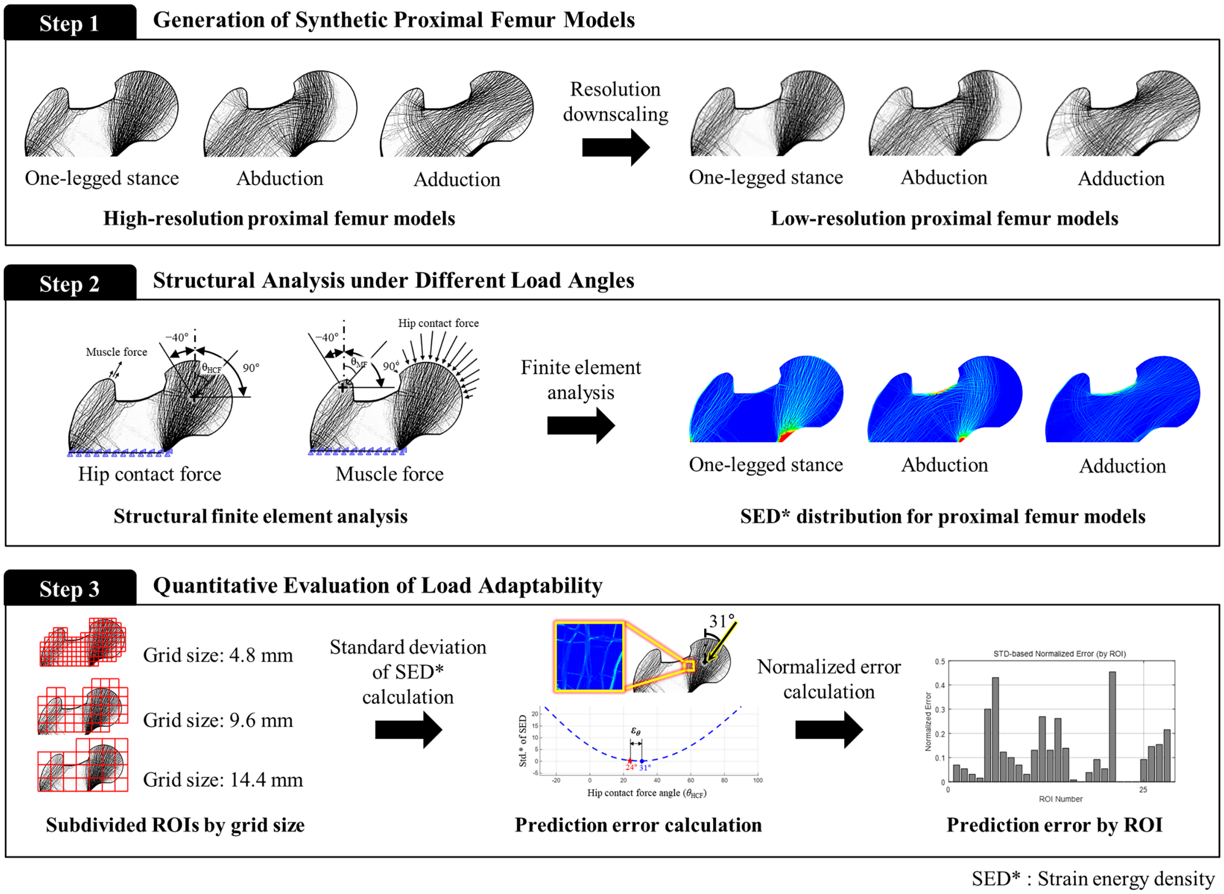

**Figure 1:** Overview of optimality assessment and structural analysis of interest regions under applied load in the proximal femur.

### 2.1 Generation of Synthetic Proximal Femur Models

Three types of 2D FE models of the synthetic proximal femur were generated to quantitatively evaluate the structural optimality under different model resolutions and loading conditions. The process comprised two steps: (i) generation of a topology optimization-based 2D FE model, and (ii) downscaling to obtain a low-resolution (LR) model.

In the topology optimization-based 2D model generation step, a bone remodeling method [31] based on topology optimization was applied to construct high-resolution (HR; 50 μm) 2D synthetic proximal femur models under three loading conditions. This method, based on the mathematical relationship between the metabolic process of bone remodeling and topology optimization, reconstructs optimal trabecular bone microstructures under given loading conditions. In this study, an initial FE model of the bone microstructure was created to obtain the optimal bone microstructure under the three loading cases, as shown in Fig. 2a. The FE model was built using 1,312,666 elements, each being a square element of 50 μm × 50 μm (width × height). All the elements in the uniform material models were assumed to be 2D square elements, and the PLANE42 element (bi-linear Lagrange four-node element) from ANSYS APDL (a commercial FEA program) was utilized. The initial trabecular bone structure was represented by a randomly generated hollow circular pattern, a modeling approach validated by Adachi et al. [34,35]. The following material properties were assigned: an elastic modulus of 22.5 GPa for the cortical bone, an elastic modulus of 15.0 GPa [36] for the trabecular bone, and a Poisson's ratio of 0.3 [36]. Considering the biomechanical characteristics of the proximal femur, which is exposed to various loading conditions during daily activities, three representative loading cases (one-legged stance, abduction, and adduction) were adopted, as suggested by Beaupré et al. [37,38] and widely employed in studies on bone remodeling and structural adaptability [4–7]. As illustrated in Fig. 2a, three synthetic proximal femur models were generated under these loading scenarios and were subsequently used in the analysis. Loads were applied as distributed forces on the femoral surface, each with a distinct magnitude and direction of the resultant force. For the boundary conditions, all the degrees of freedom at the distal part of the femur were constrained.

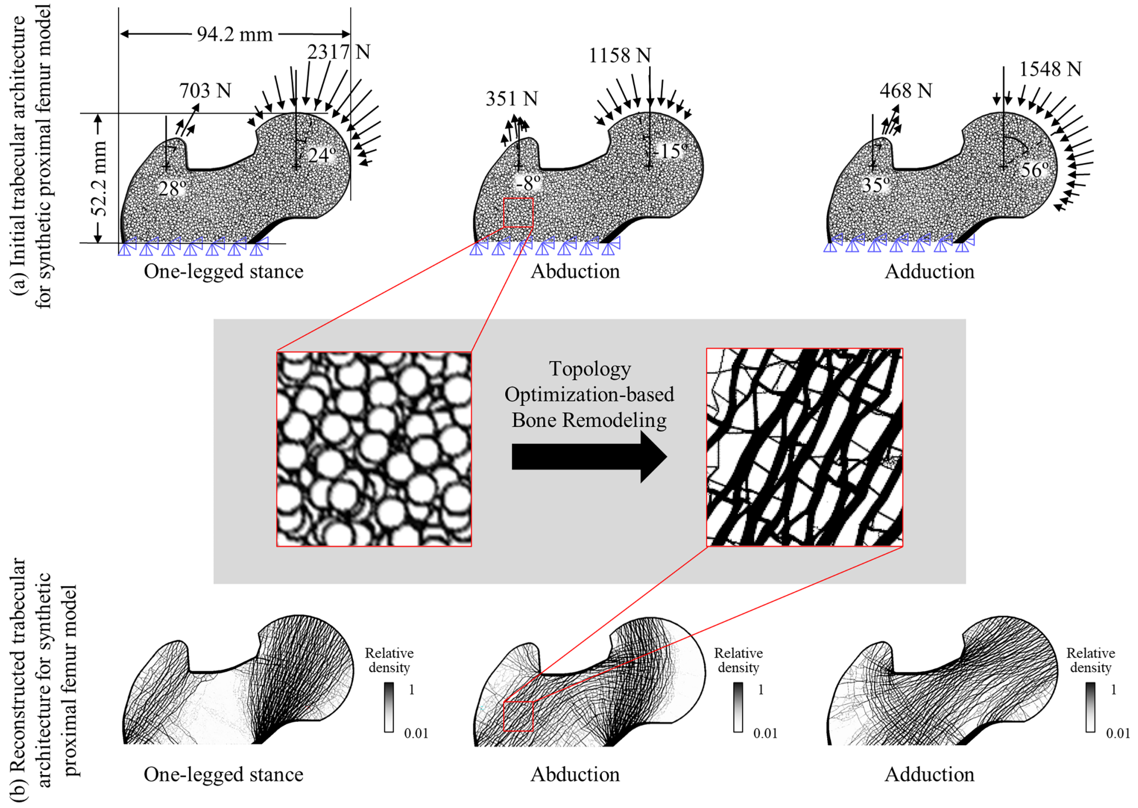

**Figure 2:** Initial trabecular architecture and 2D synthetic human proximal femur model.

The topology-optimization-based bone remodeling method [31] iteratively updates the bone distribution according to Wolff's law [15]. With this approach, the bone microstructure evolves into an optimal structure under applied loads. The optimization objective is set to minimize the strain energy under the given loads, subject to mass and perimeter constraints. The topology optimization process can be mathematically formulated as follows:

$$\begin{aligned} &\text{Miminize} \quad f(\boldsymbol{\rho}) = \tfrac{1}{2}\mathbf{u}^T\mathbf{K}\mathbf{u} \\ &\textit{Subject to} \quad g_1(\boldsymbol{\rho}) = \sum_{i=1}^{N} \boldsymbol{\rho}_i v_i \le M_0, \\ &\qquad\qquad\quad g_2(\boldsymbol{\rho}) = P \ge P_0 \end{aligned} \tag{1}$$

here, $f(\boldsymbol{\rho})$ denotes the compliance, $\mathbf{u}$ is the displacement under the given load, and $\mathbf{K}$ is the stiffness matrix. $\boldsymbol{\rho}$ is the design variable representing the density of each element, ranging from 0.001 (bone marrow) to 1 (fully dense bone). $N$ is the number of FEs, $v$ is the volume of each element, and $M_0$ is the total mass constraint of the bone. $P$ and $P_0$ denote the perimeter under the given load and the perimeter constraint, respectively. Through topology optimization, three HR (50 μm) synthetic proximal femur models were generated, as illustrated in Fig. 2b. In Ansys 2024 R1 (Ansys, Inc., Canonsburg, PA, USA), the finite element (FE) equation system was solved using the preconditioned conjugate gradient (PCG) algorithm [39], and the optimization procedure was carried out with the method of moving asymptotes (MMA) [40]. All FE simulations were executed on a workstation with an Intel(R) Core™ i9-10900K processor (3.70 GHz) and 128 GB RAM. Further methodological details are available in [31].

In the LR model generation step, additional models were created to quantitatively analyze the influence of resolution differences on the load optimality prediction. Specifically, as shown in Fig. 3a, the HR model was partitioned into $n \times n$ element clusters, and the average density of each cluster was computed and replaced by a single element. In this study, $n = 12$ was used to construct an LR synthetic proximal femur model with a resolution of 600 μm. As illustrated in Fig. 3b, LR (600 μm) synthetic proximal femur models were generated for each loading condition, while preserving the structural conformity of the original HR (50 μm) models.

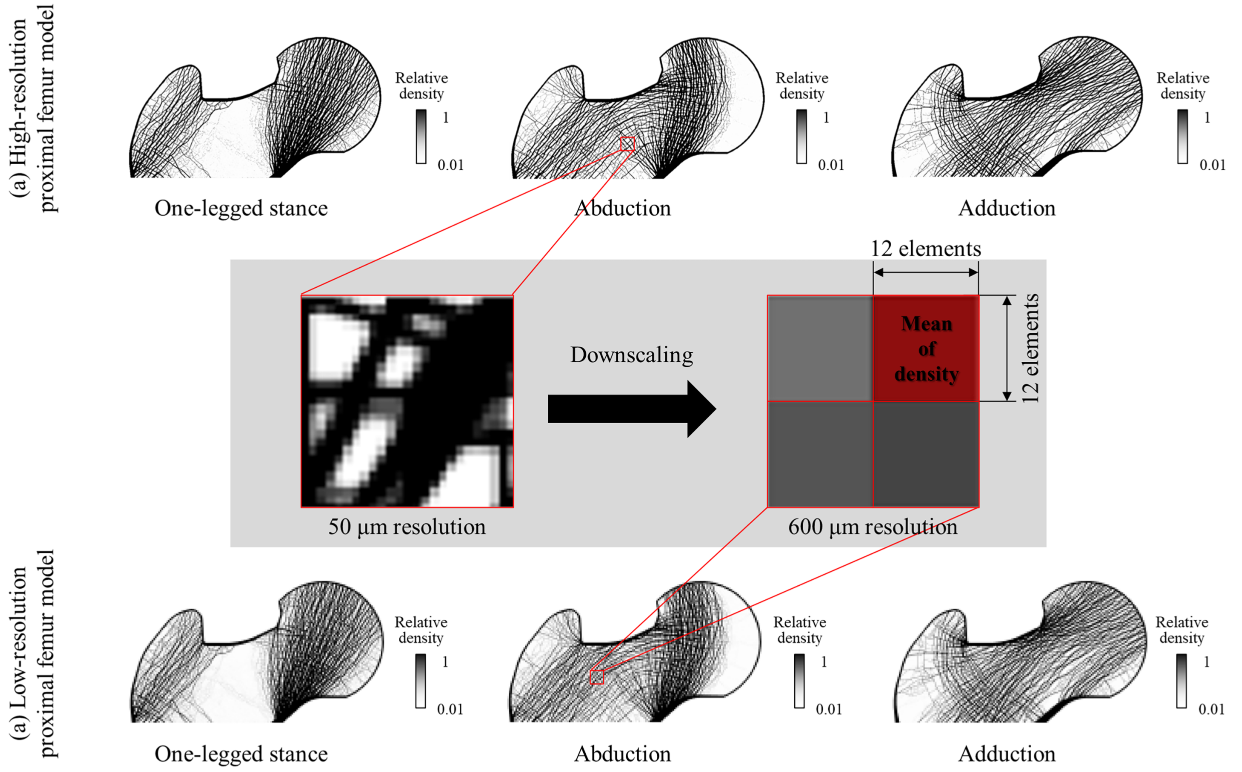

**Figure 3:** Resolution reduction from high- to low-resolution proximal femur models.

### *2.2 Region-of-Interest-Based Structural Analysis*

In the ROI-based structural analysis step, structural analyses were performed using three synthetic proximal femur models under various loading conditions. As shown in Fig. 4, the distal part of the femur is fully constrained. The loading conditions comprised musculoskeletal system-based global loads (HCF and MF) applied as distributed loads on the femoral head and greater trochanter, respectively. Each applied load was defined by the magnitude and direction of the resulting distributed force. The loading angles of the HCF and MF were independently varied in increments of 1° to evaluate the load adaptability. Specifically, both the HCF and MF were varied within a range of −40° to 90°, with the upper and lower limits set to encompass the physiological range of normal bone conditions [41]. This angular sweep was defined to systematically evaluate the sensitivity of regional structural responses to loading orientation. Representative biomechanical studies report that normal hip motion in the frontal plane during functional activities includes abduction of approximately 10°–45° and adduction of approximately 10° to 30° [42]. The selected range therefore includes this physiological motion range while providing additional margin for directional sensitivity analysis. In addition, previous studies have shown that the magnitude and orientation of hip joint contact forces vary across daily activities and muscle activation patterns [43,44]. The magnitudes of the HCF and MF were adopted from predefined values. All the FE analyses were conducted using ANSYS 2024 R1 (APDL) on a workstation (Intel(R) Core™ i9-10900K processor (3.70 GHz) and 128 GB RAM).

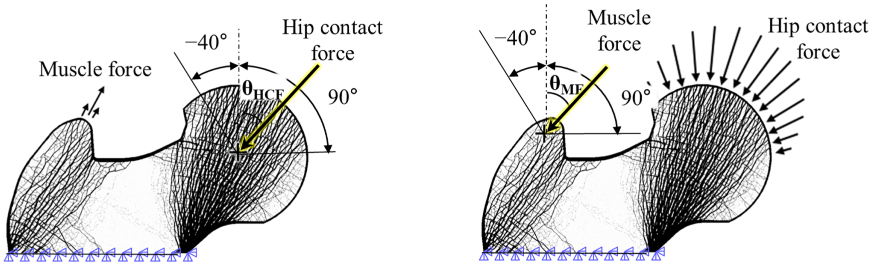

(a) Boundary conditions for hip contact force angle variation

(b) Boundary conditions for muscle force angle variation

**Figure 4:** Boundary conditions for hip contact force and muscle force angle variations.

### *2.3 Quantitative Evaluation of Load Adaptability*

Following the completion of the structural analyses, we post-processed the results by subdividing the model into grids to quantitatively evaluate the load adaptability across the ROIs. As illustrated in Fig. 5, three different grid sizes (4.8, 9.6, and 14.4 mm) were applied to the same model to investigate the influence of the ROI size on load adaptability. To evaluate the influence of ROI size on regional structural metrics, three grid sizes (4.8, 9.6, and 14.4 mm) were applied to the same proximal femur model. These scales represent small, intermediate, and large ROIs and were selected to assess the sensitivity of the conformity index to ROI size and to examine the stability of regional structural responses across different ROI scales. The numbers of ROIs were 220, 60, and 28, respectively, with region indices assigned sequentially from lower left to right and then from bottom to top. This post-processing procedure enabled the comparison and evaluation of the load adaptability with respect to the anatomical location and ROI size within the proximal femur.

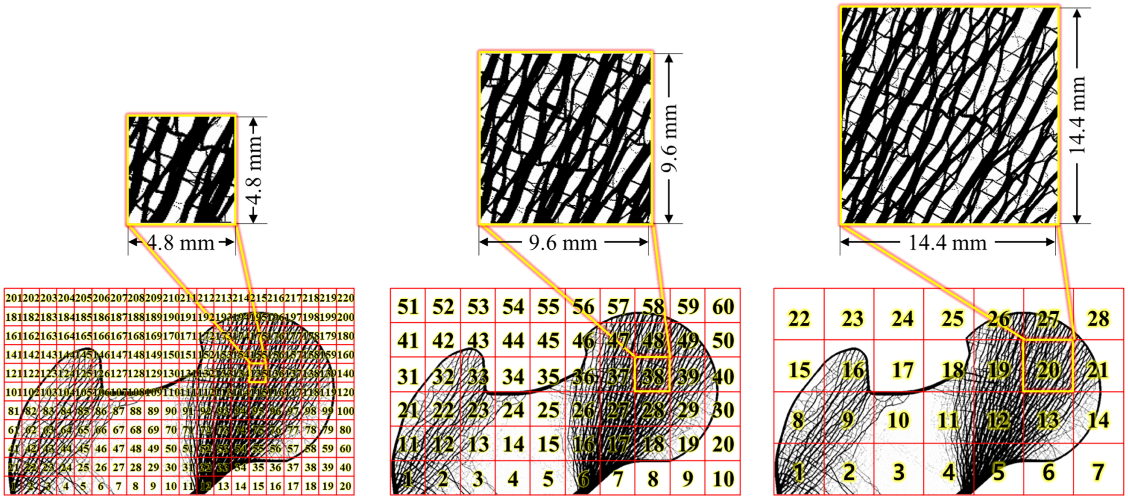

(a) Subdivided ROIs of the proximal femur model with 4.8 mm grid size

(b) Subdivided ROIs of the proximal femur model with 9.6 mm grid size

(c) Subdivided ROIs of the proximal femur model with 14.4 mm grid size

**Figure 5:** Subdivision of regions of interest (ROIs) in the proximal femur model with grid sizes of 4.8, 9.6, and 14.4 mm.

The load adaptability was quantitatively evaluated by comparing the conformity between the predicted loading angle and reference loading angles in each ROI based on the SED distributions obtained from the structural analysis. To this end, the standard deviation ($\sigma_{SED}$) of the SED distribution in each ROI under varying loading conditions was first calculated, as defined in Eq. (2) and illustrated in Fig. 6a.

$$\sigma_{SED} = \sqrt{\frac{1}{n}\sum_{i=1}^{n}\left(SED_i - \mu_{SED}\right)^2}, \tag{2}$$

here, $\sigma_{SED}$ denotes the standard deviation of the SED distribution within each ROI, $n$ is the number of elements in the ROI, $SED_i$ is the strain energy density of each element, and $\mu_{SED}$ represents the mean SED of all the elements within the ROI. Since the load adaptability of a structure tends to occur in a manner that minimizes differences in the strain energy [45–47], the angle at which the standard deviation is minimized among multiple loading angles was defined as the predicted loading angle ($\theta_{pred}$), as illustrated in Fig. 6a. The predicted loading angle ($\theta_{pred}$) was then compared with the reference loading angle ($\theta_{ref}$) to evaluate the conformity, and this procedure was repeated for all ROIs to enable comparisons of the load adaptability across regions.

The error between the predicted and reference angles was normalized using Eq. (3).

$$\varepsilon_\theta = \frac{\left|\theta_{pred} - \theta_{ref}\right|}{\theta_{\max} - \theta_{\min}}, \tag{3}$$

here, $\varepsilon_\theta$ represents the normalized prediction error of the loading angle, $\theta_{pred}$ is the predicted loading angle, and $\theta_{ref}$ is the reference loading angle. $\theta_{\max}$ and $\theta_{\min}$ indicate the maximum and minimum values of the applied loading angle range, respectively. Subsequently, each normalized error was calculated for each region of interest (ROI) and summarized as a histogram by ROI, as shown in Fig. 6b.

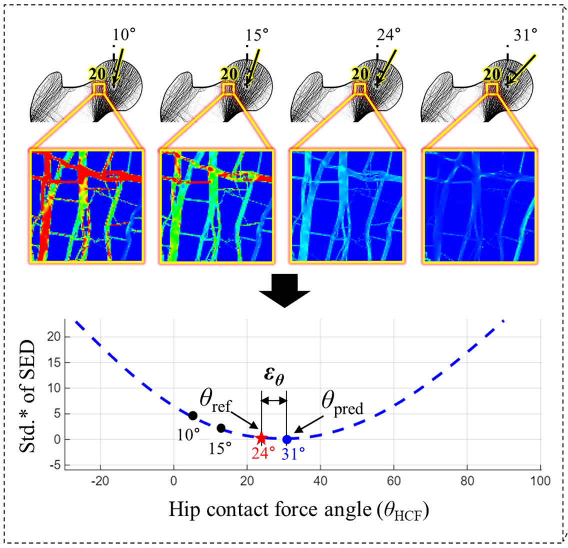

Std.* : Standard deviation

(a) Prediction error between the reference and predicted load angle

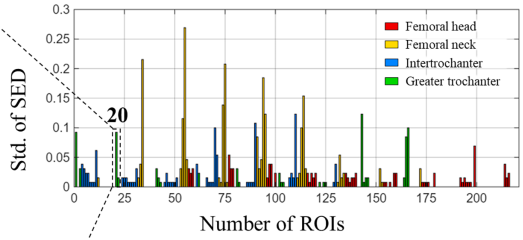

(b) Normalized error between predicted and reference load angle for ROIs

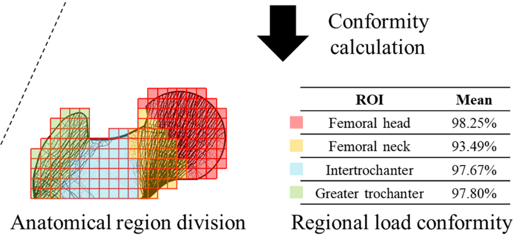

| ROI | Mean |
|---|---|
| 🟥 Femoral head | 98.25% |
| 🟨 Femoral neck | 93.49% |
| 🟦 Intertrochanter | 97.67% |
| 🟩 Greater trochanter | 97.80% |

(c) Regional load conformity

**Figure 6:** Quantitative evaluation of load adaptability based on SED-derived predicted load angle and conformity index.

A lower normalized error indicates higher adaptability of the trabecular microstructure within the ROI to the applied loading, whereas a higher error indicates lower adaptability. Based on this definition, the conformity index was introduced as a quantitative indicator of load adaptability. The conformity index is defined in Eq. (4).

$$C_\theta = 100 - \varepsilon_\theta, \tag{4}$$

here, $C_\theta$ denotes the conformity index representing the degree of agreement between the predicted and reference loading angles, where higher values indicate a greater level of conformity. Thus, the conformity index $C_\theta$ serves as a direct quantitative measure of the load adaptability at the ROI level, enabling a systematic evaluation and comparison of the region-specific structural adaptability of the proximal femur. In this study, the conformity index was computed using trabecular bone elements within each ROI grid in order to quantify trabecular load-adaptability characteristics. For the analysis of regional conformity patterns, the proximal femur was further divided into four anatomical regions: femoral head, femoral neck, intertrochanteric region, and greater trochanter, with grid sizes of 4.8, 9.6, and 14.4 mm as shown in Fig. 7a–c. Furthermore, as shown in Fig. 6c, the conformity values of individual ROIs within each anatomical region were averaged to obtain the mean conformity for each region. To enable region-wise comparison, the same model geometry, ROI definition, and numerical procedure were maintained for all simulations, and only the loading direction was systematically varied.

### *2.4 Numerical Robustness Analysis (Resolution and ROI-Size)*

To quantitatively assess the numerical robustness of the conformity index $C_\theta$ with respect to model resolution and ROI size, additional robustness metrics were calculated based on the conformity values obtained under the same loading conditions and ROI definitions described in Section 2.3. Specifically, robustness was evaluated under the three loading conditions (one-legged stance, abduction, and adduction), two model resolutions (HR: 50 μm; LR: 600 μm), and three ROI sizes (4.8, 9.6, and 14.4 mm) for each anatomical region (femoral head, femoral neck, intertrochanteric region, and greater trochanter), as illustrated in Fig. 7a–c.

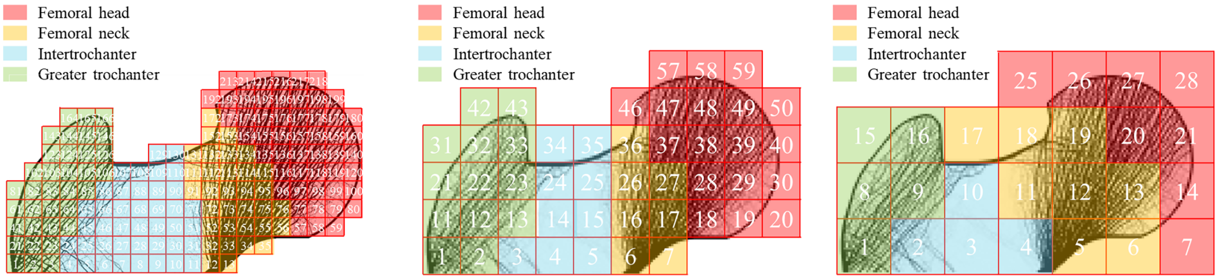

(a) Anatomical region division of the proximal femur with 4.8 mm grid size

(b) Anatomical region division of the proximal femur with 9.6 mm grid size

(c) Anatomical region division of the proximal femur with 14.4 mm grid size

**Figure 7:** Anatomical region division of the proximal femur with different grid sizes (4.8, 9.6, and 14.4 mm).

First, the sensitivity of $C_\theta$ to model resolution was evaluated by computing the resolution-dependent difference between HR and LR predictions, defined as

$$\Delta C_\theta = C_{\theta,HR} - C_{\theta,LR}, \tag{5}$$

here, $\Delta C_\theta$ denotes the change in conformity attributable to the resolution difference under the same loading condition and ROI definition. Because both decreases and minor increases may occur depending on the ROI and loading condition, the magnitude of the resolution effect was summarized using $|\Delta C_\theta|$. Subsequently, for each anatomical region, the mean and maximum values of $|\Delta C_\theta|$ across all loading conditions and ROI sizes were calculated to identify both the overall sensitivity and the worst-case sensitivity to resolution.

Second, the robustness of $C_\theta$ with respect to ROI size was evaluated by quantifying the variability of conformity across the three ROI sizes. To this end, the range of $C_\theta$ across ROI sizes (4.8–14.4 mm) was first computed as $\max(C_\theta) - \min(C_\theta)$, where the maximum and minimum were taken across the three ROI sizes under a fixed loading condition and resolution. The relative variability was then expressed as the normalized range ($NR$),

$$NR\,(\%) = 100 \times \frac{\max(C_\theta) - \min(C_\theta)}{mean\,(C_\theta)}, \tag{6}$$

where $mean\,(C_\theta)$ represents the mean conformity across the three ROI sizes. Here, a lower $NR$ indicates that the conformity estimate is less affected by ROI-size changes (i.e., higher numerical stability), regardless of whether $C_\theta$ increases monotonically with ROI size. Finally, the mean and maximum $NR$ values across the three loading conditions were calculated for each anatomical region, separately for HR and LR, to summarize ROI-size robustness.

## 3 Results

By comparing the conformity between the reference and predicted loading angles across the ROIs, we found clear differences in the load adaptability of the proximal femur depending on the ROI. Tables 1 and 2 present the conformity indices with respect to variations in the HCF and MF angles, respectively, indicating the degree of load adaptability. In the high-resolution model (ROI size 4.8 mm) under HCF-one-legged stance, the femoral head exhibited the highest conformity (98.25%), indicating excellent structural adaptability. The femoral neck showed the lowest conformity, with an average of 93.80%; in particular, cortical bone–dominant ROI 55 exhibited the lowest conformity of 73.08%. The intertrochanteric region and the greater trochanter maintained high conformity, with errors of only 2.33% and 2.20%, respectively. By contrast, under the abduction model, the greater trochanter exhibited the highest conformity (92.04%), whereas the femoral head (77.45%), femoral neck (79.50%), and intertrochanteric region (78.14%) all showed similar, lower levels of adaptability. Under the adduction model, conformity values were approximately 90% across all regions, indicating little regional variation. These results demonstrate that the load adaptability of the proximal femur varies depending on both anatomical location and loading condition, with certain regions responding more sensitively to specific load cases.

**Table 1:** Regional load conformity under hip contact force with respect to ROI size, image resolution, and model type (one-legged stance, abduction, and adduction).

| **Image Resolution** | **ROI Size** | **ROI** | **Type of Synthetic Proximal Femur Model** | | |
|---|---|---|---|---|---|
| | | | **One-Legged Stance** | **Abduction** | **Adduction** |
| High resolution | 4.8 mm | Femoral head | 98.25% | 92.20% | 91.89% |
| | | Femoral neck | 93.49% | 71.75% | 92.96% |
| | | Intertrochanter | 97.67% | 78.50% | 90.92% |
| | | Greater trochanter | 97.80% | 68.88% | 91.08% |
| | 9.6 mm | Femoral head | 97.52% | 91.20% | 93.68% |
| | | Femoral neck | 95.82% | 75.05% | 93.08% |
| | | Intertrochanter | 97.21% | 79.52% | 90.48% |
| | | Greater trochanter | 98.33% | 70.90% | 92.05% |
| | 14.4 mm | Femoral head | 98.02% | 96.37% | 93.08% |
| | | Femoral neck | 96.81% | 84.51% | 93.41% |
| | | Intertrochanter | 98.27% | 76.15% | 92.12% |
| | | Greater trochanter | 99.54% | 75.23% | 91.23% |
| Low resolution | 4.8 mm | Femoral head | 76.07% | 79.98% | 76.94% |
| | | Femoral neck | 75.19% | 52.76% | 86.61% |
| | | Intertrochanter | 95.13% | 70.04% | 83.85% |
| | | Greater trochanter | 88.26% | 63.47% | 85.6% |
| | 9.6 mm | Femoral head | 77.18% | 80.90% | 83.72% |
| | | Femoral neck | 82.09% | 50.55% | 91.32% |
| | | Intertrochanter | 97.09% | 70.77% | 82.79% |
| | | Greater trochanter | 89.49% | 65.71% | 87.05% |
| | 14.4 mm | Femoral head | 80.33% | 79.56% | 79.56% |
| | | Femoral neck | 80.11% | 65.38% | 89.34% |
| | | Intertrochanter | 96.73% | 65.96% | 86.54% |
| | | Greater trochanter | 92.31% | 65.69% | 90.46% |

**Table 2:** Regional load conformity under muscle force with respect to ROI size, image resolution, and model type (one-legged stance, abduction, and adduction).

| Image Resolution | ROI Size | ROI | Type of Synthetic Proximal Femur Model | | |
|---|---|---|---|---|---|
| | | | One-Legged Stance | Abduction | Adduction |
| High resolution | 4.8 mm | Femoral head | 60.00% | 55.58% | 65.06% |
| | | Femoral neck | 87.19% | 75.48% | 73.08% |
| | | Intertrochanter | 96.17% | 77.77% | 82.58% |
| | | Greater trochanter | 97.41% | 88.09% | 85.91% |
| | 9.6 mm | Femoral head | 63.33% | 60.94% | 65.30% |
| | | Femoral neck | 95.82% | 78.68% | 75.93% |
| | | Intertrochanter | 96.83% | 77.88% | 84.13% |
| | | Greater trochanter | 99.04% | 89.81% | 88.14% |
| | 14.4 mm | Femoral head | 55.60% | 58.79% | 59.45% |
| | | Femoral neck | 87.47% | 77.80% | 76.37% |
| | | Intertrochanter | 95.96% | 74.81% | 83.65% |
| | | Greater trochanter | 99.54% | 92.62% | 84.62% |
| Low resolution | 4.8 mm | Femoral head | 54.73% | 47.88% | 64.26% |
| | | Femoral neck | 60.62% | 65.58% | 66.73% |
| | | Intertrochanter | 90.38% | 72.00% | 73.68% |
| | | Greater trochanter | 80.20% | 80.02% | 77.01% |
| | 9.6 mm | Femoral head | 55.56% | 50.51% | 63.76% |
| | | Femoral neck | 62.42% | 72.42% | 70.44% |
| | | Intertrochanter | 93.75% | 68.85% | 73.08% |
| | | Greater trochanter | 85.58% | 77.76% | 80.26% |
| | 14.4 mm | Femoral head | 50.66% | 45.82% | 65.38% |
| | | Femoral neck | 64.07% | 65.49% | 65.27% |
| | | Intertrochanter | 87.31% | 71.54% | 77.12% |
| | | Greater trochanter | 87.23% | 82.31% | 83.69% |

In terms of the MF results, analysis based on subdivision into 4.8 mm × 4.8 mm ROIs revealed that the greater trochanter exhibited the highest adaptability with a conformity of 97.41% (error 2.59%). The intertrochanteric region, femoral neck, and femoral head followed with conformity values of 96.17%, 87.19%, and 60.00%, respectively. Thus, the order of conformity from highest to lowest was greater trochanter, intertrochanteric region, femoral neck, femoral head. A Similar ranking was observed in the abduction and adduction models with the same ROI size. These findings indicate that the load adaptability to MF in the proximal femur is highest in ROIs closest to the applied force and lowest in those located farther away.

A comparison of the load conformity with respect to the model resolution revealed that the LR model exhibited an overall lower conformity than the HR model. Figs. 8 and 9 show histograms of prediction errors across ROIs under HCF and MF one-legged stance models, respectively, indicating that the distribution shifted upward in the low-resolution model, corresponding to increased error (results for adduction and abduction models are presented in Figs. A1–A4). As shown in Table 3, for HCF-one-legged

(ROI 4.8 mm), conformity in the femoral head decreased from 98.25% to 76.07% (−22.18%p), whereas the femoral neck, greater trochanter, and intertrochanteric region decreased by 18.30%p, 9.54%p, and 2.54%p, respectively. Under HCF-abduction, the femoral neck decreased by 18.99%p, whereas under HCF-adduction the femoral head and greater trochanter decreased by 14.95%p and 5.48%p, respectively. In MF-one-legged (ROI 4.8 mm), the femoral neck decreased from 87.19% to 60.62%, corresponding to a reduction of 26.57%p (Table 2). Overall, conformity in the low-resolution model decreased by between 2.54%p and 26.57%p, with the femoral head and femoral neck identified as the regions most sensitive to resolution changes.

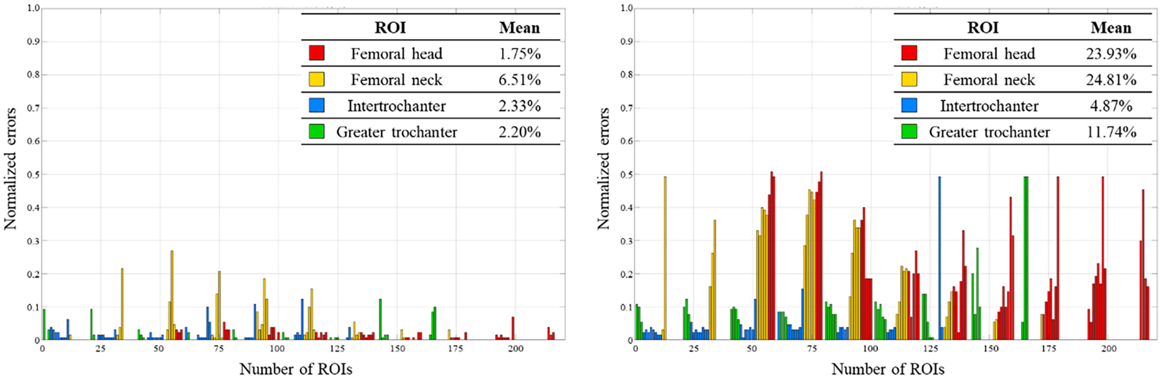

(a) High-resolution model with 4.8 mm ROI size (b) Low-resolution model with 4.8 mm ROI size

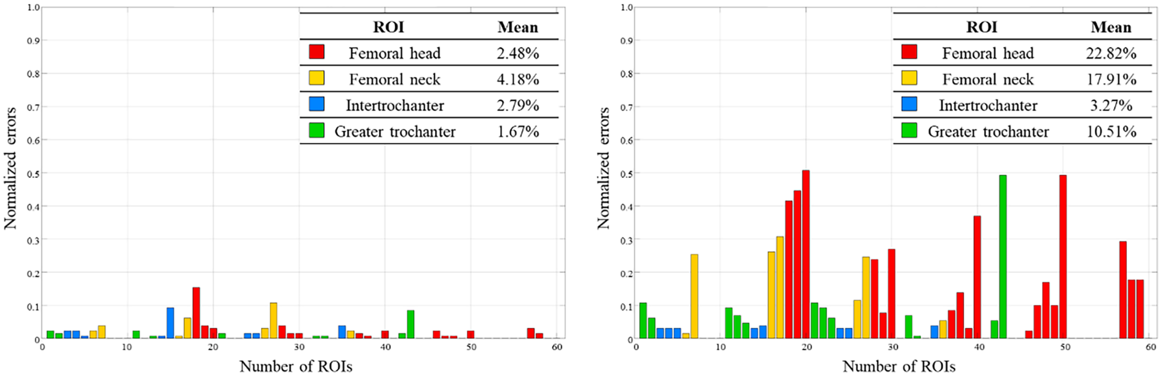

(c) High-resolution model with 9.6 mm ROI size (d) Low-resolution model with 9.6 mm ROI size

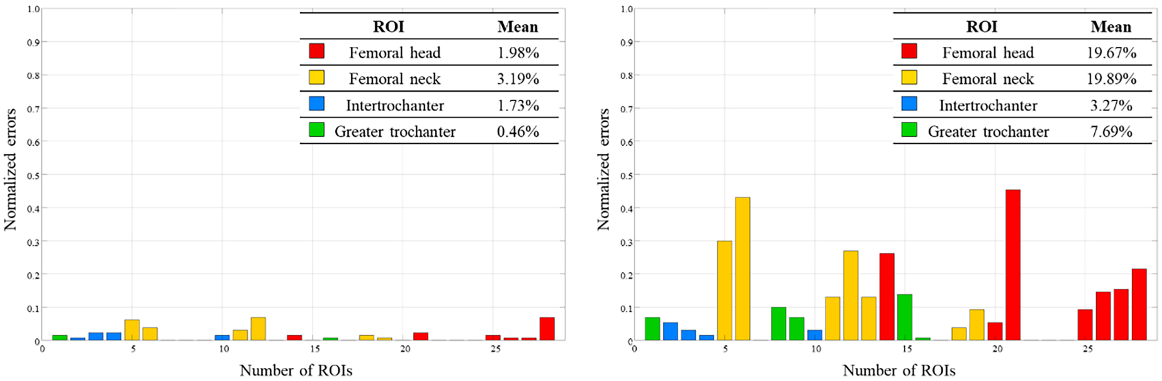

(e) High-resolution model with 14.4 mm ROI size (f) Low-resolution model with 14.4 mm ROI size

**Figure 8:** Histogram of normalized error between predicted and reference load angles in ROIs under hip contact force for the one-legged stance model.

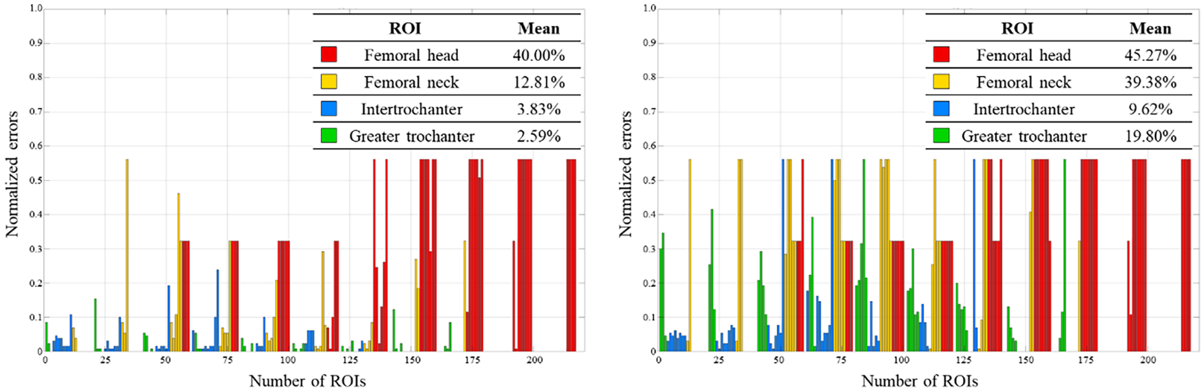

(a) High-resolution model with 4.8 mm ROI size (b) Low-resolution model with 4.8 mm ROI size

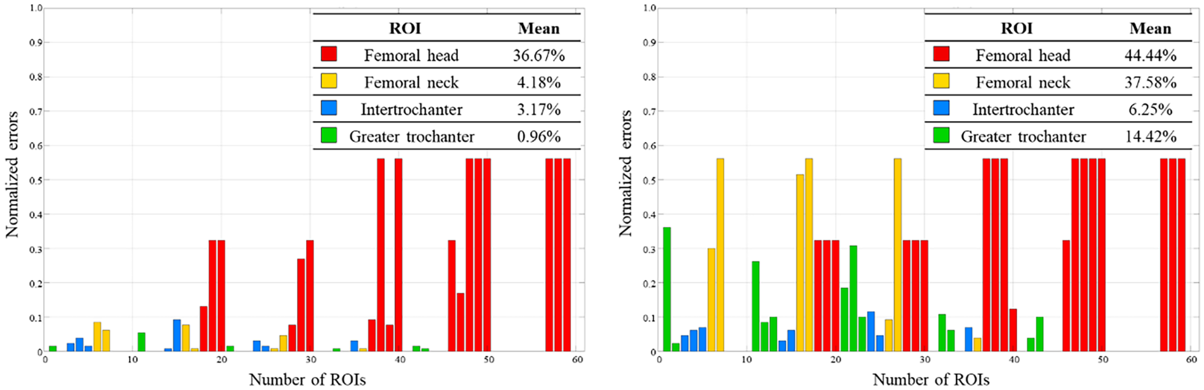

(c) High-resolution model with 9.6 mm ROI size (d) Low-resolution model with 9.6 mm ROI size

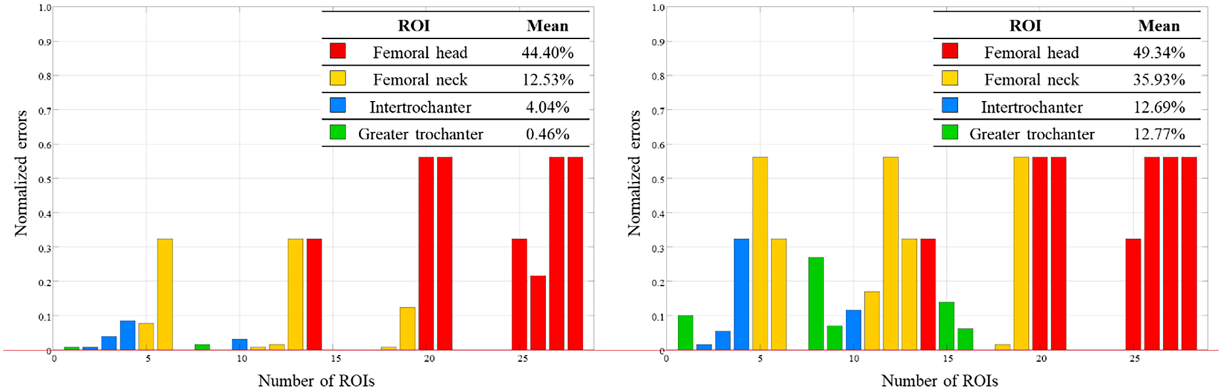

(e) High-resolution model with 14.4 mm ROI size (f) Low-resolution model with 14.4 mm ROI size

**Figure 9:** Histogram of normalized error between predicted and reference load angles in ROIs under muscle force for the one-legged stance model.

When comparing prediction accuracy according to loading condition, conformity was highest in the one-legged stance, followed by adduction, and lowest in abduction (Table 1). In the high-resolution HCF-one-legged stance model, the femoral head and greater trochanter exhibited the highest conformity at 98.25% and 97.80%, respectively. Under HCF-adduction, all regions showed conformity values of approximately 90%, slightly lower than in the one-legged stance, but still relatively high. In contrast, HCF-abduction exhibited the lowest conformity overall, with the femoral neck and greater trochanter at 71.75% and 68.88%, respectively. Under MF loading, conformity was also highest in the one-legged stance model (average approximately 94%), followed by the adduction model (approximately 90%) and the abduction model (approximately 88%) (Table 2). In summary, across all loading conditions, conformity was consistently highest in the one-legged stance model and lowest in the abduction model.

**Table 3:** Resolution sensitivity of the conformity index with respect to model resolution.

| Force Type | ROI | Mean ($\lvert\Delta C_\theta\rvert$) [%p] | Max ($\lvert\Delta C_\theta\rvert$) [%p] | Max at: Model, ROI Size |
|---|---|---|---|---|
| HCF | Femoral head | 15.33 | 22.18 | One-legged stance, 4.8 mm |
| | Femoral neck | 13.73 | 24.50 | Abduction, 9.6 mm |
| | Intertrochanter | 5.77 | 10.19 | Abduction, 14.4 mm |
| | Greater trochanter | 6.33 | 9.54 | Abduction, 14.4 mm |
| MF | Femoral head | 6.37 | 12.97 | Abduction, 14.4 mm |
| | Femoral neck | 14.98 | 33.40 | One-legged stance, 9.6 mm |
| | Intertrochanter | 6.90 | 11.05 | Adduction, 9.6 mm |
| | Greater trochanter | 10.12 | 17.21 | One-legged stance, 4.8 mm |

When comparing conformity according to ROI size, larger ROIs consistently yielded higher conformity across all loading conditions (Table 1). In HCF-one-legged, femoral neck conformity increased from 93.49% at 4.8 mm to 95.82% at 9.6 mm and 96.81% at 14.4 mm. In HCF-adduction, femoral neck conformity increased from 92.96% (4.8 mm) to 93.08% (9.6 mm) and 93.41% (14.4 mm). In HCF-abduction, femoral neck conformity was lowest at 71.75% (4.8 mm) but increased to 75.05% (9.6 mm) and 84.51% (14.4 mm). Thus, conformity generally improved as ROI size increased, with the femoral neck—initially showing the lowest values at small ROIs—also exhibiting higher conformity at larger ROIs. In contrast, the low-resolution model did not exhibit consistent improvement with increasing ROI size. In HCF-one-legged, femoral neck conformity increased from 75.19% (4.8 mm) to 82.09% (9.6 mm), but decreased again to 80.11% at 14.4 mm. In HCF-abduction, conformity was lowest at 4.8 mm (71.75%) but steadily increased to 83.49% (9.6 mm) and 85.72% (14.4 mm). Therefore, unlike the high-resolution model, the low-resolution model showed irregular patterns in conformity with ROI size, while maintaining lower absolute values across all conditions (Table 1).

Numerical robustness of the conformity index $C_\theta$ was evaluated with respect to model resolution and ROI size using the metrics defined in Section 2.4. Resolution sensitivity, expressed as $\lvert\Delta C_\theta\rvert = \lvert C_{\theta,HR} - C_{\theta,LR}\rvert$, revealed the largest worst-case deviation in the femoral neck (max $\lvert\Delta C_\theta\rvert$ = 24.50% for HCF and 33.40% for MF), whereas the intertrochanteric region exhibited consistently smaller deviations across loading conditions (Table 3). ROI-size robustness was assessed using the normalized range $NR$ (%), which quantifies the variability of $C_\theta$ across the three ROI sizes. The largest variability was observed in the femoral neck under HCF conditions (LR $NR_{\max}$ = 26.37%), whereas the femoral head showed the largest average variability under MF conditions (HR $NR_{mean}$ = 10.46%) (Table 4). Overall, these robustness metrics consistently indicate that the femoral neck is the most resolution- and ROI-size-sensitive region, whereas the intertrochanteric region exhibits comparatively stable numerical behavior across modeling conditions. These results indicate that prediction stability is better interpreted in terms of variability with respect to ROI size rather than a strictly monotonic increase of $C_\theta$ with increasing ROI size. The interaction patterns across resolution, ROI size, and loading condition are illustrated in Appendix B.

**Table 4:** ROI-size robustness of the conformity index quantified using the normalized range (NR).

| Force Type | ROI | High Resolution | | | Low Resolution | | |
|---|---|---|---|---|---|---|---|
| | | $NR_{mean}$ [%] | $NR_{\max}$ [%] | Max at Model | $NR_{mean}$ [%] | $NR_{\max}$ [%] | Max at Model |
| HCF | Femoral head | 2.74 | 5.54 | Abduction | 5.20 | 8.47 | Adduction |
| | Femoral neck | 6.84 | 16.55 | Abduction | 13.46 | 26.37 | Abduction |
| | Intertrochanter | 2.40 | 4.32 | Abduction | 4.49 | 6.98 | Abduction |
| | Greater trochanter | 3.90 | 8.86 | Abduction | 4.50 | 5.54 | Adduction |
| MF | Femoral head | 10.46 | 12.96 | One-legged stance | 7.13 | 9.76 | Abduction |
| | Femoral neck | 6.03 | 9.57 | One-legged stance | 7.80 | 10.22 | Abduction |
| | Intertrochanter | 2.25 | 4.00 | Abduction | 5.66 | 7.12 | One-legged stance |
| | Greater trochanter | 3.75 | 5.02 | Abduction | 7.45 | 8.34 | One-legged stance |

## 4 Discussion

We first quantitatively analyzed the structural response characteristics and load adaptability of the proximal femur. The results showed that, even under identical loading conditions, the femoral head and greater trochanter exhibited high conformity, whereas the femoral neck showed low conformity, indicating region-specific differences with respect to local anatomical features. Furthermore, a reduction in the model resolution significantly affected the predictive accuracy, with the femoral neck being the most sensitive region, while the intertrochanteric area remained relatively stable. Depending on the loading conditions, a high conformity was maintained under localized concentrated loads; however, the predictive accuracy decreased when stresses were more widely distributed. The ROI size was another important factor influencing interregional variability. Small ROIs were advantageous for capturing local responses, whereas large ROIs were more effective in ensuring stability and reproducibility. These findings are consistent with previous results—the anatomical structure, model resolution, loading conditions, and ROI size influence the reliability of FEM-based analyses. Moreover, this study quantitatively demonstrated that these four factors were the key determinants of the structural adaptability of the proximal femur under loading.

Our quantitative analysis confirmed that the structural responsiveness varied across ROIs within the proximal femur, even under identical loading conditions. In the present two-dimensional analysis, the conformity results are interpreted primarily as comparative ROI-wise trends; therefore, the following results are discussed in terms of regional differences under controlled changes in loading direction [48]. Based on the HR model with an ROI size of 4.8 mm under the one-legged stance condition, the femoral head exhibited the highest conformity, with a mean value of 98.25%, whereas the greater trochanter and intertrochanter maintained high conformity values of 97.80% and 97.67%, respectively. In contrast, the femoral neck showed the lowest mean conformity of 93.49%, and particularly in the cortical bone-dominant regions, the conformity dropped to as low as 73.08%. These differences indicate that the femoral head, as a direct load-transfer pathway of joint compressive forces, has high structural adaptability to the HCF [49–51], whereas the femoral neck, which is least influenced by the HCF, demonstrated lower structural adaptability [20,52,53]. This suggests that while the trabeculae in the femoral neck contribute to reinforcement and stress distribution, they are not the primary load-bearing structures [54,55] and that conformity is primarily governed by the cortical bone strength in this region. Under MF conditions, the greater trochanter showed the highest conformity, with a mean value of 97.41%, followed by the intertrochanter at 96.17%. This finding is consistent with those of previous studies [20,52,53] that reported that the greater trochanter, as a major muscle attachment site, directly responds to muscle loading. In the present study, this influence was further observed to extend into the intertrochanteric region. By contrast, the femoral head and neck exhibited relatively lower conformity under MF conditions, suggesting that these regions are more strongly influenced by joint compressive loads than by MFs. These regional differences align with recent structural models proposing that the proximal femur has triangular and arch-based mechanical characteristics [22,23]. The triangular structure formed by the superior, medial, and lateral cortical walls efficiently distributes the joint compressive loads, whereas the trabecular alignment along the arch-shaped framework provides mechanical stability by alternately supporting compressive and tensile forces. The high conformity observed in the femoral head and greater trochanter, the low conformity in the femoral neck, and the intermediate conformity in the intertrochanter quantitatively demonstrate how this arch-based load transfer mechanism manifests in actual structural responses. In conclusion, the proximal femur structurally adapts to mechanical loading; however, the femoral responses to HCFs and MFs are distinctly differentiated in terms of the local anatomy and loading patterns. SED has frequently been adopted as a mechanical stimulus in computational studies of bone adaptation and remodeling. Classical mechanoregulation theories propose that trabecular architecture evolves in response to the mechanical environment so that the internal mechanical stimulus approaches a regulated state [45,46]. Based on this concept, several computational studies have used SED-based measures to investigate trabecular bone adaptation and load-driven structural responses [48,56,57]. From this perspective, the conformity index used in the present study can be interpreted as a regional descriptor of how uniformly mechanical energy is distributed within a trabecular structure under different loading orientations. Accordingly, the CI reflects the relative adaptability of trabecular architecture to different loading directions rather than representing a universal criterion of structural optimality.

This study quantitatively confirmed that changes in the load conformity due to differences in model resolution varied across ROIs in the femur. Compared with the HR model (50 μm), the LR model (600 μm) exhibited a predominant tendency toward reduced conformity, with minor exceptions in specific combinations of ROI, loading condition, and ROI size, as shown in Figs. 7 and 8. Based on regional conformity values, in the HCF scenario, changes ranged from a minimum increase of 0.12% in the intertrochanteric ROI of the one-legged stance model with 9.6 mm ROIs to a maximum decrease of 24.5% in the femoral neck ROI of the abduction model with 9.6 mm ROIs. A similar trend was observed in the MF scenario, where under one-legged stance conditions, the femoral neck ROI showed the highest reduction in conformity, up to 33.4%. These results demonstrate that the femoral neck is the most sensitive ROI to model resolution changes in both the HCF and MF models. In contrast, the intertrochanteric ROI maintained a relatively stable conformity despite the resolution differences, showing the lowest sensitivity. These findings are consistent with those of previous studies [58] that reported that a lower model resolution underestimates or distorts the stress concentration and strain distribution, thereby markedly reducing the predictive accuracy of the load response. Furthermore, by capturing the numerical differences in the conformity, this study quantitatively demonstrated that the femoral neck ROI was the most resolution-dependent, whereas the intertrochanteric ROI maintained a relatively stable conformity.

The predictive accuracy of structural optimality under different loading conditions improved when the applied load was more localized but reduced when it was more widely distributed. Under the one-legged stance condition, the femoral head and femoral neck exhibited conformity values of approximately 98.25% and 93.49%, respectively, indicating a very high accuracy. As shown in Fig. 10a, this results from the concentrated transmission of the hip joint contact load to the femoral head and neck, leading to locally high conformity. In contrast, under the abduction condition, the conformities of the femoral neck and greater trochanter decreased to approximately 71.75% and 68.88%, respectively, falling below 70%, as illustrated in Fig. 10b, where stresses are more widely distributed in the intertrochanteric region and greater trochanter, leading to reduced local conformity. The adduction condition exhibited an intermediate trend: as shown in Fig. 10c, the femoral head maintained a conformity of 91.89%, while the other regions also maintained a conformity of 90%, which was lower than that under the one-legged stance condition. A similar trend was observed under MF loading, where the one-legged stance model showed the highest accuracy with a conformity of 97.41% in the greater trochanter, whereas the adduction model showed the lowest at 85.91% (Fig. 10d–f). These findings suggest that conformity serves as a key indicator in explaining structural responses; more localized loading results in higher conformity, whereas more distributed loading results in lower conformity. This is consistent with previous studies that reported that under complex and distributed loading conditions, such as sideways falls [59], the lateral femoral neck exhibited prediction errors of approximately 30%, the highest among the regions. In other words, simple localized loading conditions preserve the predictive accuracy, whereas multiaxial and distributed loadings, such as falls, can cause a sharp decline in the conformity of specific regions. Therefore, this study quantitatively demonstrated that the differences in conformity under varying loading conditions are not merely numerical changes but represent fundamental alterations in the structural response patterns of the proximal femur depending on whether the applied load is localized or distributed.

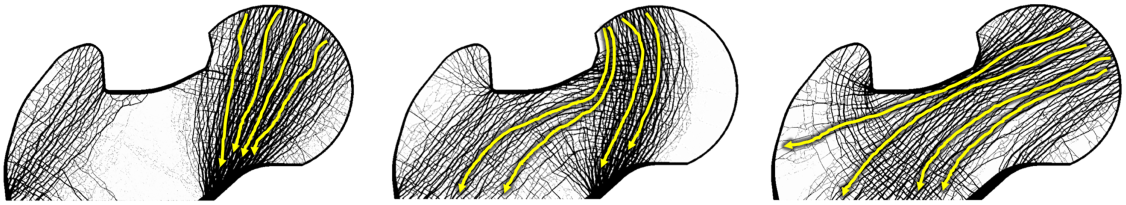

(a) Hip contact force transfer path in the one-legged stance model

(b) Hip contact force transfer path in the abduction model

(c) Hip contact force transfer path in the adduction model

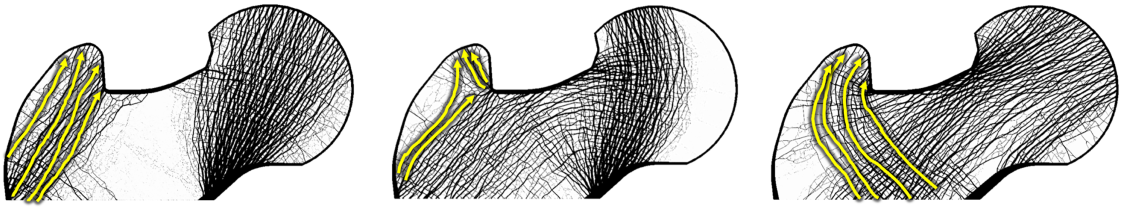

(d) Muscle force transfer path in the one-legged stance model

(e) Muscle force transfer path in the abduction model

(f) Muscle force transfer path in the adduction model

**Figure 10:** Principal load transfer pathways of hip contact force and muscle forces in the proximal femur under one-legged stance, abduction, and adduction models.

A comparison of the predictive accuracy across different ROI sizes revealed that, overall, larger ROIs yielded higher conformity and improved the stability of the results. Smaller ROIs (e.g., 4.8 mm) often included anatomical boundaries, such as the cortical–trabecular junction or regions with large structural variations, where local element-level differences were strongly reflected. Consequently, conformity showed greater variability and lower mean values. For example, under the one-legged stance condition, the femoral neck with a 4.8 mm ROI exhibited a conformity of 93.49%, which was lower than those of the other regions. In contrast, when the ROI size was increased to 9.6 and 14.4 mm, broader anatomical structures were encompassed, averaging out microstructural heterogeneity. Consequently, conformity was maintained more stably, and interregional deviations decreased to 4.18% and 3.19%, respectively. This suggests that while small ROIs are advantageous for detecting local variations, larger ROIs are more suitable for ensuring consistency and reliability in the overall load adaptability assessment. These findings are consistent with computed tomography quality control studies [60], which reported that maintaining an ROI above a certain size is essential for accurate noise measurements, highlighting that the ROI size is not a simple technical parameter but a crucial factor determining the reproducibility and reliability of the results. Previous studies have reported that the selected ROI volume can influence trabecular microarchitectural parameters. For example, Wen et al. [61] showed that insufficient ROI volume in the femoral head can significantly affect measured trabecular parameters. In addition, proximal femur trabecular studies have commonly employed ROIs with dimensions of several millimeters; for instance, Munemoto et al. [62] defined cylindrical ROIs with a diameter of approximately 5 mm in the femoral head for trabecular microstructure analysis. Consistent with these findings, our previous trabecular reconstruction study based on topology optimization [63] also showed that decreasing ROI size increased variability in trabecular morphometric indices, particularly in the femoral neck region. Taken together with the present results, these observations indicate that ROI size should be carefully considered when evaluating regional structural metrics. In particular, relatively larger ROIs may provide more stable conformity values when the objective is regional comparison rather than detection of highly localized variations. The robustness analysis further clarifies how discretization choices influence the conformity index $C_\theta$. The metrics summarized in Tables 3 and 4 indicate that prediction stability is most appropriately interpreted through variability measures, specifically resolution sensitivity $|\Delta C_\theta|$ and ROI-size variability ($NR$), rather than through a universal monotonic increase of conformity with ROI size. This distinction is particularly relevant under MF conditions, where non-monotonic behavior of the mean $C_\theta$ with increasing ROI size can occur. Among the examined regions, the femoral neck exhibited the largest worst-case resolution sensitivity and the highest ROI-size variability under HCF conditions, suggesting that this region is most susceptible to discretization and ROI-definition effects. In contrast, the intertrochanteric region showed comparatively small $|\Delta C_\theta|$ and low $NR$ values across loading conditions, indicating greater numerical stability for trend-level interpretation. Appendix Figs. A5 and A6 provide visual confirmation of these interaction patterns.

The regional conformity patterns identified in the present study indicate that structural responsiveness of the proximal femur varies across anatomical regions depending on their role in load transfer. Specifically, the femoral head and greater trochanter exhibited higher conformity under their dominant loading conditions, whereas the femoral neck showed lower conformity, suggesting that mechanical responses are region dependent rather than uniform across the bone. This interpretation is consistent with recent computational studies on bone mechanoadaptation, which have demonstrated that bone adaptation is governed by spatially heterogeneous mechanical environments. In particular, three-dimensional finite element frameworks combined with micro-CT imaging have shown that trabecular bone formation and resorption tend to occur in region-dependent patterns associated with local mechanical stimuli [56,57]. These findings indicate that local structural characteristics and load-transfer pathways strongly influence how different anatomical regions respond to mechanical loading. Recent reviews further emphasize that contemporary bone adaptation modeling increasingly incorporates three-dimensional geometry, multiaxial loading conditions, and subject-specific musculoskeletal forces to improve the physiological realism of predicted remodeling patterns [48]. Within this broader context, the ROI-based conformity analysis used in the present study can be interpreted as a controlled regional sensitivity framework that evaluates how structural responses vary across anatomical regions under systematically varied loading orientations. Although the present analysis does not explicitly simulate long-term bone remodeling processes, the observed regional conformity trends may provide baseline insight for future studies incorporating subject-specific loading conditions and fully three-dimensional adaptive remodeling models.

This study had several limitations. First, this study was performed using a two-dimensional representation of the proximal femur. Consequently, deformation and load transfer in the thickness direction are not explicitly represented, and the detailed stress distribution and load transfer pathways may differ from those predicted by fully three-dimensional models [61]. In addition, two-dimensional analyses cannot represent the full three-dimensional structural connectivity between cortical and trabecular bone [62]. Therefore, the present results should be interpreted primarily as a comparative analysis of regional conformity patterns under controlled variations in loading direction. Nevertheless, as described in Section 2.3, because the conformity index is computed consistently across ROIs under controlled variations in loading direction, the present two-dimensional framework remains meaningful for comparative, region-specific trend identification [64]. Future studies using three-dimensional models may further refine the interpretation of regional load adaptability. Second, the loading conditions were limited to HCF and MF, without reflecting more complex and multiaxial loading scenarios. Nevertheless, by focusing on the representative loading conditions, this study identified the fundamental structural response characteristics of the proximal femur, which can be extended to future studies involving gait or falls. Third, long-term bone remodeling processes or temporal adaptation to load changes were not considered; instead, this study focused on short-term structural responses. These aspects should be addressed in future studies through time-dependent simulations. Fourth, because the conformity index was defined based on trabecular bone elements, cortical bone responses were not explicitly included in the current metric. Incorporating cortical bone measures may provide additional insights, particularly in cortical-dominant regions such as the femoral neck, and represents a potential direction for future work. Fifth, the directions of hip contact force and muscle forces were varied independently in this study. Although hip joint loading *in vivo* results from coordinated muscle activation and joint reaction forces, the independent variation adopted here provided a controlled framework for evaluating the directional sensitivity of regional structural responses. Future studies may incorporate coupled musculoskeletal loading conditions to further investigate the influence of coordinated loading interactions on regional adaptability patterns. Despite these limitations, we quantitatively demonstrated how model resolution, loading conditions, and anatomical location interact to determine the load adaptability of the proximal femur, providing baseline data for future studies involving 3D modeling and complex loading conditions.

## 5 Conclusions

This study constructed multiple 2D FE models to quantitatively evaluate the structural responses and load adaptability of the proximal femur across ROIs and compared the predictive accuracy under different loading conditions (HCF, MF), model resolutions (HR: 50 μm, LR: 600 μm), and ROI sizes (4.8–14.4 mm). The analyses revealed that, even under identical loading conditions, the femoral head and greater trochanter exhibited high conformity, whereas the femoral neck showed low conformity, indicating that local anatomical characteristics play a decisive role in load adaptability. In addition, a lower resolution consistently decreased the predictive accuracy, with the femoral neck being the most sensitive region, while the intertrochanteric region remained relatively stable. Across the loading conditions, the one-legged stance condition, in which loads are more localized, produced the highest conformity, whereas conditions, such as adduction and abduction, where stresses are more widely distributed, resulted in markedly reduced predictive accuracy. Furthermore, increasing the ROI size reduced the local variability and improved the stability of the conformity, demonstrating that the ROI size is a critical factor influencing the reliability of result interpretation. These findings are consistent with previous results—the anatomy, model resolution, loading conditions, and ROI size affect the accuracy of FEM-based analyses. By quantitatively demonstrating these effects, this study provides new evidence for understanding the structural adaptability of the proximal femur. Although limited by the 2D modeling and simplified loading conditions, our findings provide foundational insights into how ROI characteristics, model resolution, and loading conditions interact to determine structural responses, thereby supporting future 3D extensions and clinically applicable studies.

**Acknowledgement:** Not applicable.

**Funding Statement:** This research was supported by Basic Science Research Program through the National Research Foundation of Korea (NRF) funded by the Ministry of Education (No. RS-2023-00247406). This work was supported by the National Research Foundation of Korea (NRF) grant funded by the Korea government (MSIT) (No. RS-2025-00558448). We would like to acknowledge the technical support from Ansys Korea.

**Author Contributions:** Jisun Kim: formal analysis, funding acquisition, investigation, methodology, software, validation, visualization, writing—original draft. Jung Jin Kim: funding acquisition, project administration, supervision, writing—review & editing. All authors reviewed and approved the final version of the manuscript.

**Availability of Data and Materials:** Data available on request from the authors.

**Ethics Approval:** Not applicable.

**Conflicts of Interest:** The authors declare no conflicts of interest.

## Appendix A

### *Appendix A.1*

Histogram of normalized error between predicted and reference load angles in ROIs.

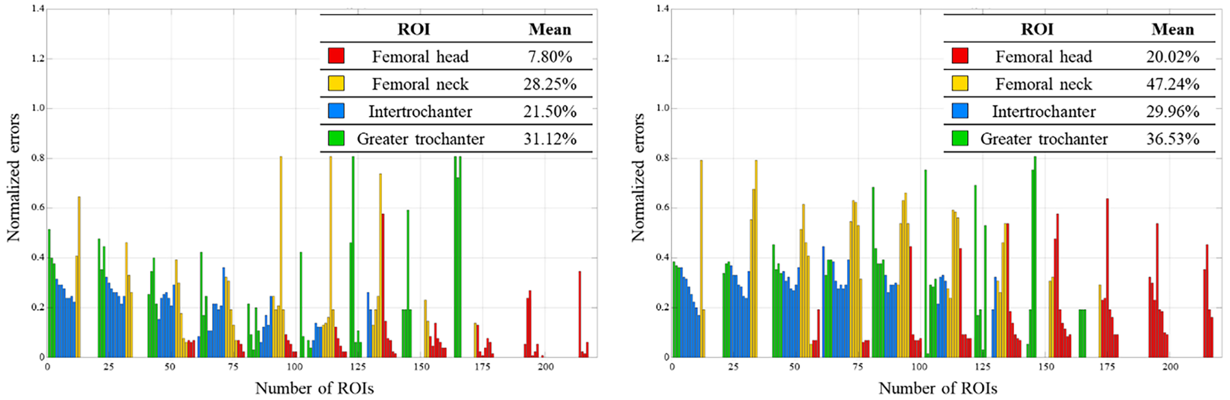

(a) High-resolution model with 4.8 mm ROI size (b) Low-resolution model with 4.8 mm ROI size

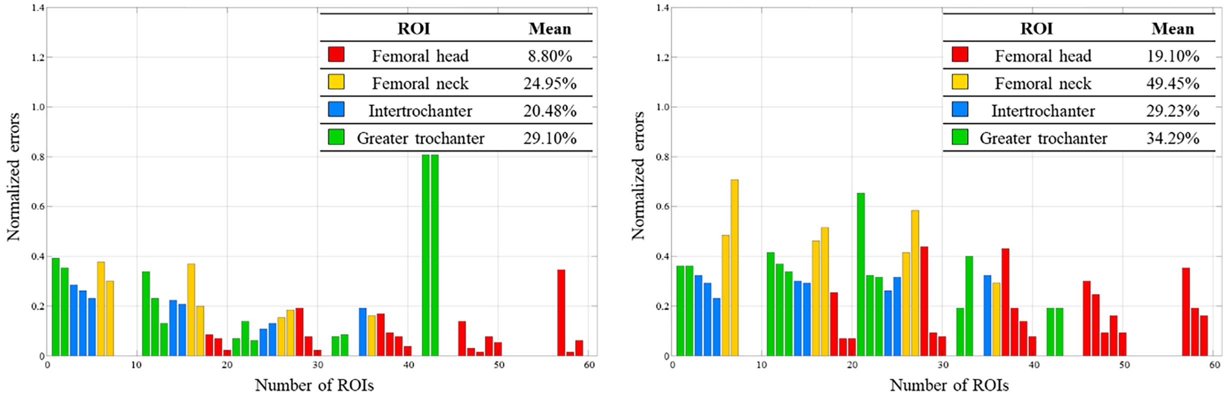

(c) High-resolution model with 9.6 mm ROI size (d) Low-resolution model with 9.6 mm ROI size

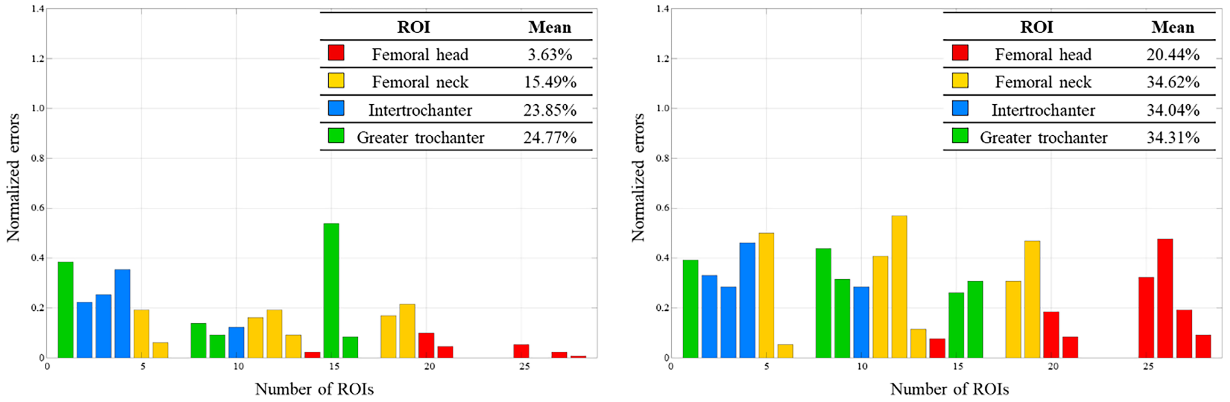

(e) High-resolution model with 14.4 mm ROI size (f) Low-resolution model with 14.4 mm ROI size

**Figure A1:** Histogram of normalized error between predicted and reference load angles in ROIs under hip contact force for the abduction model.

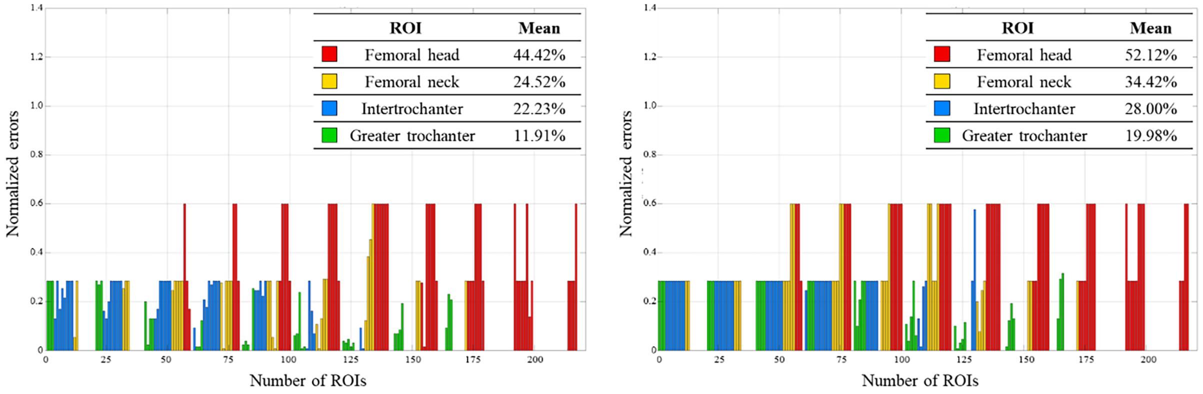

(a) High-resolution model with 4.8 mm ROI size (b) Low-resolution model with 4.8 mm ROI size

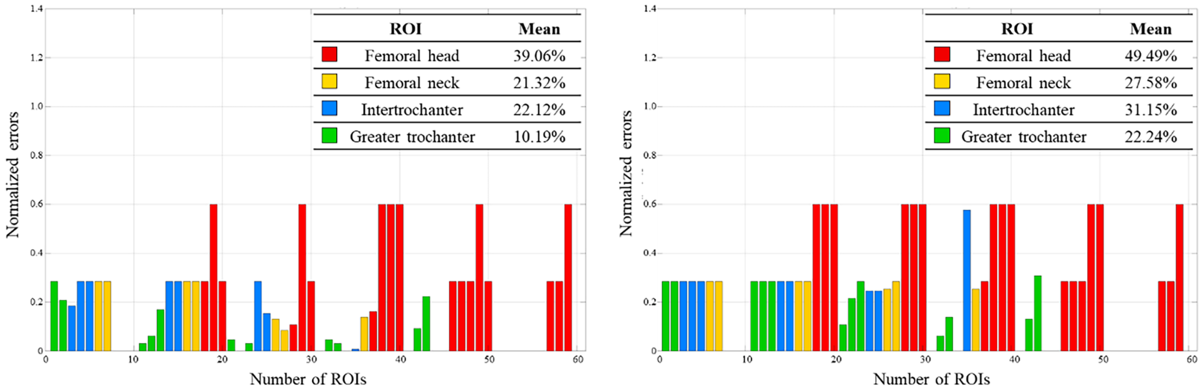

(c) High-resolution model with 9.6 mm ROI size (d) Low-resolution model with 9.6 mm ROI size

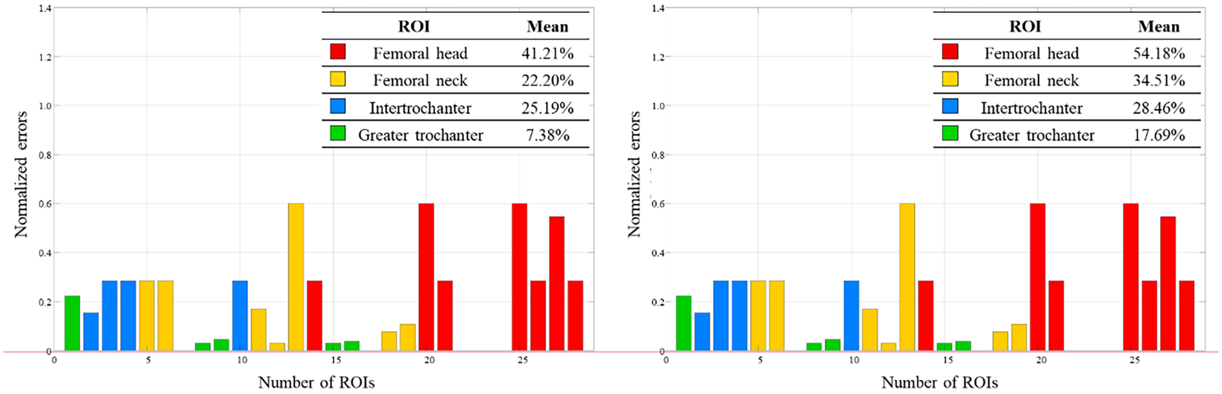

(e) High-resolution model with 14.4 mm ROI size (f) Low-resolution model with 14.4 mm ROI size

**Figure A2:** Histogram of normalized error between predicted and reference load angles in ROIs under muscle force for the abduction model.

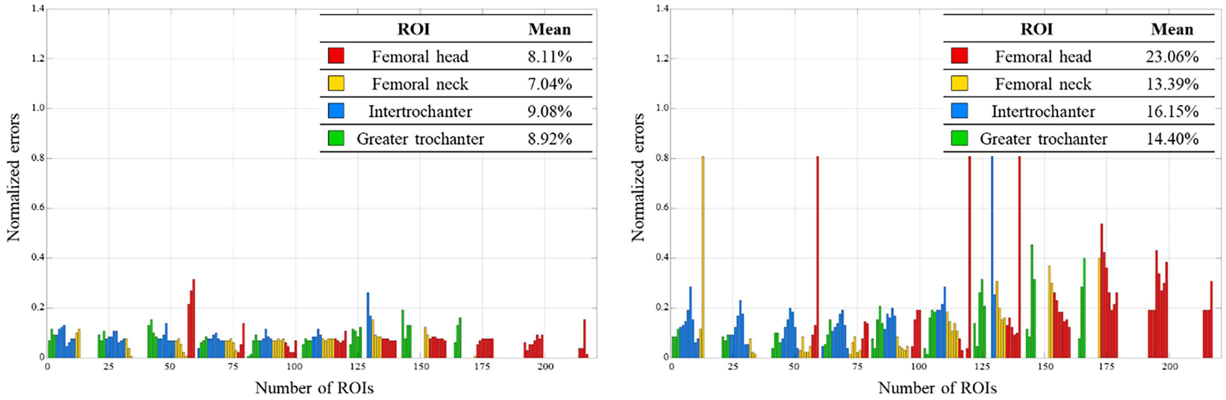

(a) High-resolution model with 4.8 mm ROI size (b) Low-resolution model with 4.8 mm ROI size

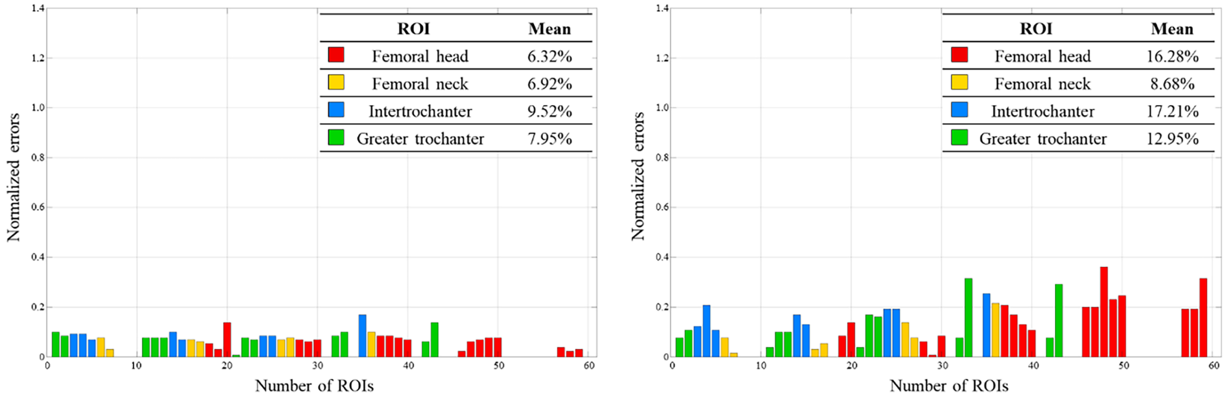

(c) High-resolution model with 9.6 mm ROI size (d) Low-resolution model with 9.6 mm ROI size

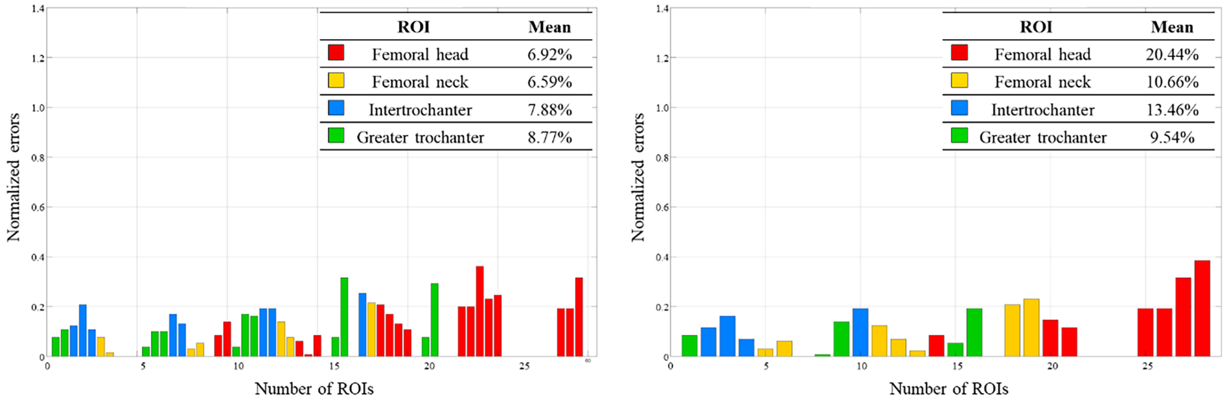

(e) High-resolution model with 14.4 mm ROI size (f) Low-resolution model with 14.4 mm ROI size

**Figure A3:** Histogram of normalized error between predicted and reference load angles in ROIs under hip contact force for the adduction model.

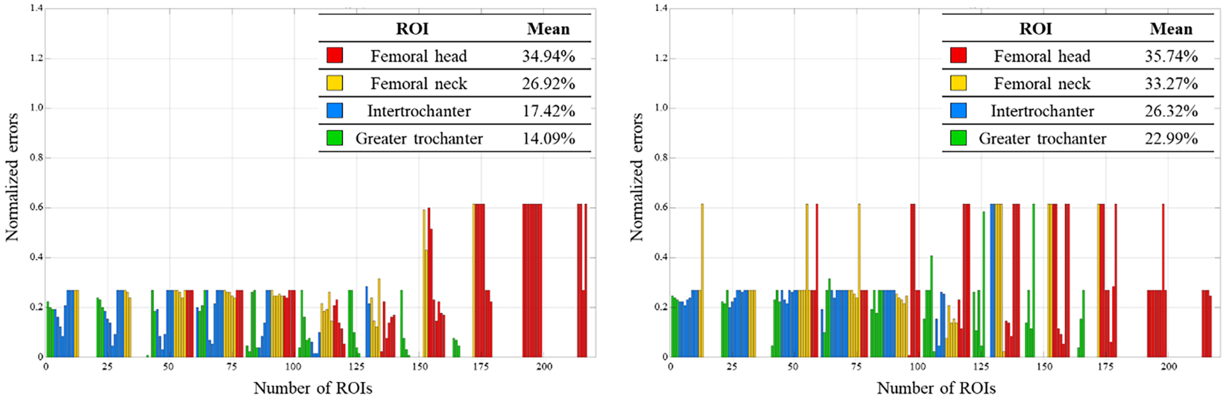

(a) High-resolution model with 4.8 mm ROI size (b) Low-resolution model with 4.8 mm ROI size

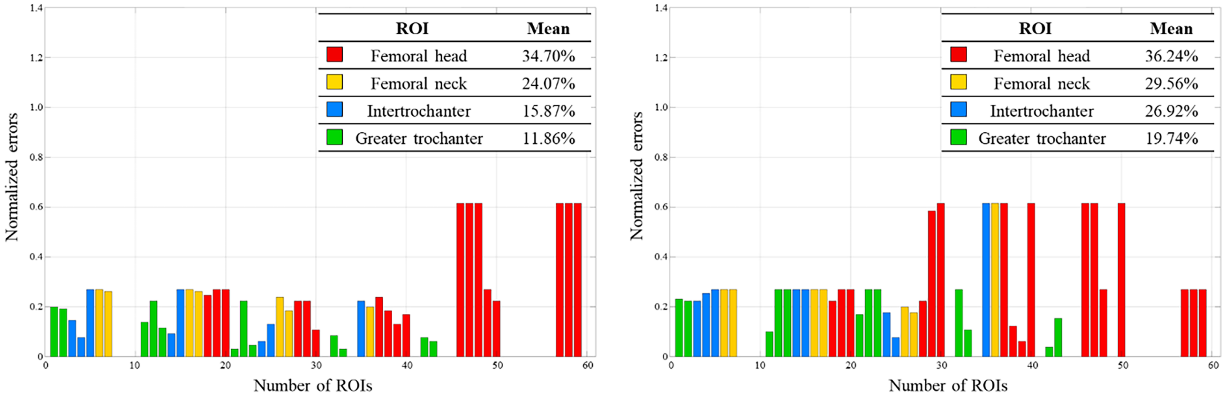

(c) High-resolution model with 9.6 mm ROI size (d) Low-resolution model with 9.6 mm ROI size

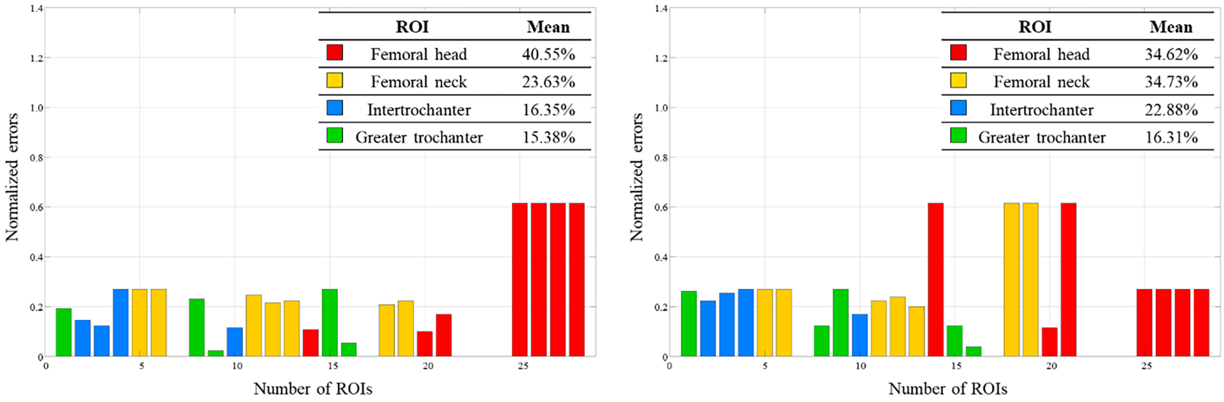

(e) High-resolution model with 14.4 mm ROI size (f) Low-resolution model with 14.4 mm ROI size

**Figure A4:** Histogram of normalized error between predicted and reference load angles in ROIs under muscle force for the adduction model.

## Appendix B

### *Appendix B.1*

Interaction plots for numerical robustness of the conformity index with respect to ROI size and model resolution.

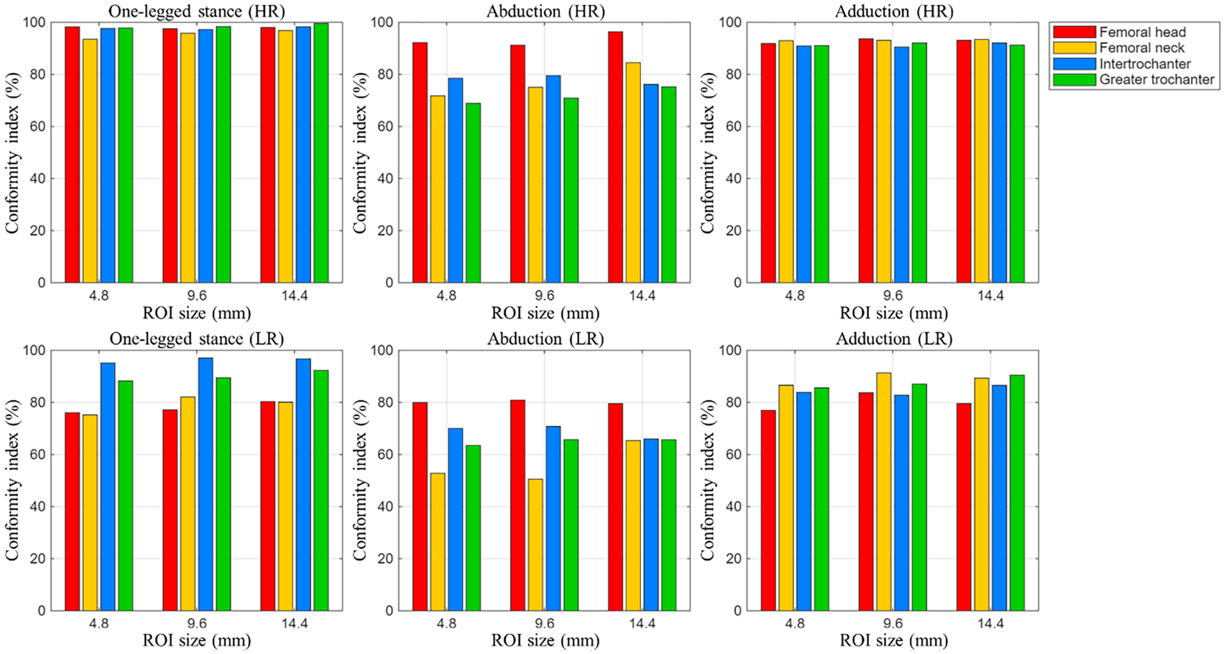

**Figure A5:** Interaction plots for numerical robustness of the conformity index with respect to ROI size, model resolution, and loading condition.

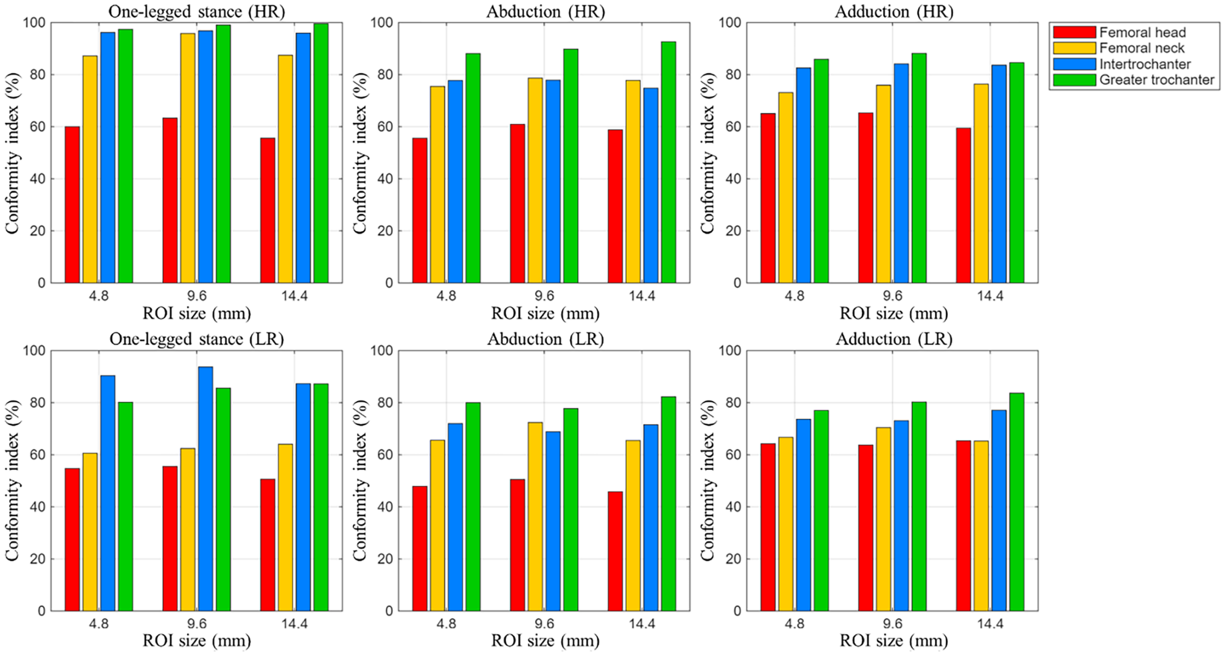

**Figure A6:** Interaction plots of the conformity index as a function of ROI size under muscle force (MF), showing the effects of loading conditions, model resolution, and femoral regions of interest.

## References

1. Sas A, Sermon A, van Lenthe GH. Experimental validation of a voxel-based finite element model simulating femoroplasty of lytic lesions in the proximal femur. Sci Rep. 2022;12(1):7602. doi:10.1038/s41598-022-11667-x.

2. Hollensteiner M, Baumeister D, Mühling M, Greinwald M, Sandriesser S, Hofstätter B, et al. Population-specific femur models: a step towards improved osteosynthetic biomechanical testing in orthopaedics. Clin Biomech. 2025;121(Suppl. 2):106379. doi:10.1016/j.clinbiomech.2024.106379.
3. Qasim M, López Picazo M, Ruiz Wills C, Noailly J, Di Gregorio S, Del Río Barquero LM, et al. 3D-DXA based finite element modelling for femur strength prediction: evaluation against QCT. J Clin Densitom. 2024;27(2):101471. doi:10.1016/j.jocd.2024.101471.
4. Kim JJ, Jang IG. Image resolution enhancement for healthy weight-bearing bones based on topology optimization. J Biomech. 2016;49(13):3035–40. doi:10.1016/j.jbiomech.2016.06.012.
5. Kim JJ, Kim Y, Jang IG. Estimation of local bone loads for the volume of interest. J Biomech Eng. 2016;138(7):071004. doi:10.1115/1.4033478.
6. Jang IG, Kim IY. Application of design space optimization to bone remodeling simulation of trabecular architecture in human proximal femur for higher computational efficiency. Finite Elem Anal Des. 2010;46(4):311–9. doi:10.1016/j.finel.2009.11.003.
7. Choi JW, Kim JJ. A computational approach to investigate the structural behavior of bone scaffold-implanted proximal femur in routine clinical resolution. Int J Numer Methods Biomed Eng. 2025;41(7):e70072. doi:10.1002/cnm.70072.
8. Turner CH. Three rules for bone adaptation to mechanical stimuli. Bone. 1998;23(5):399–407. doi:10.1016/s8756-3282(98)00118-5.
9. Greene DA, Naughton GA. Adaptive skeletal responses to mechanical loading during adolescence. Sports Med. 2006;36(9):723–32. doi:10.2165/00007256-200636090-00001.
10. Warden SJ. Extreme skeletal adaptation to mechanical loading. J Orthop Sports Phys Ther. 2010;40(3):188. doi:10.2519/jospt.2010.0404.
11. Willie BM, Zimmermann EA, Vitienes I, Main RP, Komarova SV. Bone adaptation: safety factors and load predictability in shaping skeletal form. Bone. 2020;131(10):115114. doi:10.1016/j.bone.2019.115114.
12. Geraldes DM, Modenese L, Phillips ATM. Consideration of multiple load cases is critical in modelling orthotropic bone adaptation in the femur. Biomech Model Mechanobiol. 2016;15(5):1029–42. doi:10.1007/s10237-015-0740-7.
13. Verhulp E, van Rietbergen B, Huiskes R. Load distribution in the healthy and osteoporotic human proximal femur during a fall to the side. Bone. 2008;42(1):30–5. doi:10.1016/j.bone.2007.08.039.
14. Hazra A, Chanda S, Chakraborty D. Orthotropic characterization of trabecular bone remodeling in human femur: a biomechanical study. Proc Inst Mech Eng Part H J Eng Med. 2025;239(9):872–84. doi:10.1177/09544119251375787.
15. Wolff J. The classic: on the significance of the architecture of the spongy substance for the question of bone growth: a preliminary publication. Clin Orthop Relat Res. 2011;469(11):3077–8. doi:10.1007/s11999-011-2041-5.
16. Safira IR, Ramette M, Masouros SD, Bull AMJ. Bone remodeling simulation using spatial influence function in macroscopic cube case. Front Bioeng Biotechnol. 2024;12:1498812. doi:10.3389/fbioe.2024.1498812.
17. Yang P, Lin TY, Xu JL, Zeng HY, Chen D, Xiong BL, et al. Finite element modeling of proximal femur with quantifiable weight-bearing area in standing position. J Orthop Surg Res. 2020;15(1):384. doi:10.1186/s13018-020-01927-9.
18. Shah MAA, Lü SJ, Zhang JF, Wang JW, Tang W, Luo WC, et al. Functional morphology of trabecular system in human proximal femur: a perspective from P45 sectional plastination and 3D reconstruction finite element analysis. J Orthop Surg Res. 2025;20(1):370. doi:10.1186/s13018-025-05773-5.
19. Amiri P, Bull AMJ. Prediction of *in vivo* hip contact forces during common activities of daily living using a segment-based musculoskeletal model. Front Bioeng Biotechnol. 2022;10:995279. doi:10.3389/fbioe.2022.995279.
20. Warden SJ, Carballido-Gamio J, Weatherholt AM, Keyak JH, Yan C, Kersh ME, et al. Heterogeneous spatial and strength adaptation of the proximal femur to physical activity: a within-subject controlled cross-sectional study. J Bone Miner Res. 2020;35(4):681–90. doi:10.1002/jbmr.3939.
21. Kim J, Chun BJ, Kim JJ. Quantitative load dependency analysis of local trabecular bone microstructure to understand the spatial characteristics in the synthetic proximal femur. Biology. 2023;12(2):170. doi:10.3390/biology12020170.

22. Xu G, Li J, Xu C, Xiong D, Li H, Wang D, et al. Triangular mechanical structure of the proximal femur. Orthop Surg. 2022;14(11):3047–60. doi:10.1111/os.13498.
23. Zhang J, Lü S, Wang J, Tang W, Li C, Campbell G, et al. The qualitative analysis of trabecular architecture of the proximal femur based on the P45 sectional plastination technique. J Anat. 2025;246(6):936–47. doi:10.1111/joa.14210.
24. Campoli G, Weinans H, Zadpoor AA. Computational load estimation of the femur. J Mech Behav Biomed Mater. 2012;10:108–19. doi:10.1016/j.jmbbm.2012.02.011.
25. Fischer KJ, Jacobs CR, Levenston ME, Cody DD, Carter DR. Bone load estimation for the proximal femur using single energy quantitative CT data. Comput Methods Biomech Bio Med Eng. 1998;1(3):233–45. doi:10.1080/01495739808936704.
26. Sass JO, Saemann M, Kebbach M, Soodmand E, Wree A, Bader R, et al. The morphology of the femur influences the fracture risk during stumbling and falls on the hip—a computational biomechanical study. Life. 2024;14(7):841. doi:10.3390/life14070841.
27. Christen P, van Rietbergen B, Lambers FM, Müller R, Ito K. Bone morphology allows estimation of loading history in a murine model of bone adaptation. Biomech Model Mechanobiol. 2012;11(3–4):483–92. doi:10.1007/s10237-011-0327-x.
28. Cao X, Keyak JH, Sigurdsson S, Zhao C, Zhou W, Liu A, et al. A new hip fracture risk index derived from FEA-computed proximal femur fracture loads and energies-to-failure. Osteoporos Int. 2024;35(5):785–94. doi:10.1007/s00198-024-07015-6.
29. Heřt J, Havránek M, Daniel M, Sosna A. Predicting proximal femoral remodeling after short-stem hip arthroplasty: a biomechanical modeling approach. J Clin Med. 2025;14(15):5307. doi:10.3390/jcm14155307.
30. Weinans H, Huiskes R, Grootenboer HJ. Effects of material properties of femoral hip components on bone remodeling. J Orthop Res. 1992;10(6):845–53. doi:10.1002/jor.1100100614.
31. Jang IG, Kim IY. Computational study of Wolff's law with trabecular architecture in the human proximal femur using topology optimization. J Biomech. 2008;41(11):2353–61. doi:10.1016/j.jbiomech.2008.05.037.
32. Coelho PG, Fernandes PR, Rodrigues HC, Cardoso JB, Guedes JM. Numerical modeling of bone tissue adaptation—a hierarchical approach for bone apparent density and trabecular structure. J Biomech. 2009;42(7):830–7. doi:10.1016/j.jbiomech.2009.01.020.
33. Mathai B, Dhara S, Gupta S. Orthotropic bone remodelling around uncemented femoral implant: a comparison with isotropic formulation. Biomech Model Mechanobiol. 2021;20(3):1115–34. doi:10.1007/s10237-021-01436-6.
34. Adachi T, Tsubota K, Tomita Y, Hollister SJ. Trabecular surface remodeling simulation for cancellous bone using microstructural voxel finite element models. J Biomech Eng. 2001;123(5):403–9. doi:10.1115/1.1392315.
35. Tsubota KI, Adachi T, Tomita Y. Functional adaptation of cancellous bone in human proximal femur predicted by trabecular surface remodeling simulation toward uniform stress state. J Biomech. 2002;35(12):1541–51. doi:10.1016/S0021-9290(02)00173-2.
36. Verhulp E, van Rietbergen B, Huiskes R. Comparison of micro-level and continuum-level voxel models of the proximal femur. J Biomech. 2006;39(16):2951–7. doi:10.1016/j.jbiomech.2005.10.027.
37. Beaupré GS, Orr TE, Carter DR. An approach for time-dependent bone modeling and remodeling-application: a preliminary remodeling simulation. J Orthop Res. 1990;8(5):662–70. doi:10.1002/jor.1100080507.
38. Beaupré GS, Orr TE, Carter DR. An approach for time-dependent bone modeling and remodeling—theoretical development. J Orthop Res. 1990;8(5):651–61. doi:10.1002/jor.1100080506.
39. Hestenes MR, Stiefel E. Methods of conjugate gradients for solving linear systems. J Res Natl Bur Stand. 1952;49(6):409–36. doi:10.6028/jres.049.044.
40. Svanberg K. The method of moving asymptotes—a new method for structural optimization. Int J Numer Methods Eng. 1987;24(2):359–73. doi:10.1002/nme.1620240207.
41. Vengust R, Daniel M, Antolič V, Zupanc O, Iglič A, Kralj-Iglič V. Biomechanical evaluation of hip joint after Salter innominate osteotomy: a long-term follow-up study. Arch Orthop Trauma Surg. 2001;121(9):511–6. doi:10.1007/s004020100282.

42. Rivière C, Vendittoli PA. Personalized hip and knee joint replacement. Cham, Switzerland: Springer; 2020. p. 350. doi:10.1007/978-3-030-24243-5.
43. Bergmann G, Deuretzbacher G, Heller M, Graichen F, Rohlmann A, Strauss J, et al. Hip contact forces and gait patterns from routine activities. J Biomech. 2001;34(7):859–71. doi:10.1016/s0021-9290(01)00040-9.
44. Lenaerts G, De Groote F, Demeulenaere B, Mulier M, Van der Perre G, Spaepen A, et al. Subject-specific hip geometry affects predicted hip joint contact forces during gait. J Biomech. 2008;41(6):1243–52. doi:10.1016/j.jbiomech.2008.01.014.
45. Huiskes R, Weinans HH, Grootenboer HJ, Dalstra M, Fudala B, Slooff TJ. Adaptive bone-remodeling theory applied to prosthetic-design analysis. J Biomech. 1987;20(11–12):1135–50. doi:10.1016/0021-9290(87)90030-3.
46. Weinans H, Huiskes R, Grootenboer HJ. The behavior of adaptive bone-remodeling simulation models. J Biomech. 1992;25(12):1425–41. doi:10.1016/0021-9290(92)90056-7.
47. Mullender MG, Huiskes R, Weinans H. A physiological approach to the simulation of bone remodeling as a self-organizational control process. J Biomech. 1994;27(11):1389–94. doi:10.1016/0021-9290(94)90049-3.
48. Meslier QA, Shefelbine SJ. Using finite element modeling in bone mechanoadaptation. Curr Osteoporos Rep. 2023;21(2):105–16. doi:10.1007/s11914-023-00776-9.
49. Kainz H, Killen BA, Wesseling M, Perez-Boerema F, Pitto L, Garcia Aznar JM, et al. A multi-scale modelling framework combining musculoskeletal rigid-body simulations with adaptive finite element analyses, to evaluate the impact of femoral geometry on hip joint contact forces and femoral bone growth. PLoS One. 2020;15(7):e0235966. doi:10.1371/journal.pone.0235966.
50. Kainz H, Koller W, Wallnöfer E, Bader TR, Mindler GT, Kranzl A. A framework based on subject-specific musculoskeletal models and Monte Carlo simulations to personalize muscle coordination retraining. Sci Rep. 2024;14(1):3567. doi:10.1038/s41598-024-53857-9.
51. Heller MO, Bergmann G, Deuretzbacher G, Claes L, Haas NP, Duda GN. Influence of femoral anteversion on proximal femoral loading: measurement and simulation in four patients. Clin Biomech. 2001;16(8):644–9. doi:10.1016/S0268-0033(01)00053-5.
52. Fuchs RK, Carballido-Gamio J, Keyak JH, Kersh ME, Warden SJ. Physical activity induced adaptation can increase proximal femur strength under loading from a fall onto the greater trochanter. Bone. 2021;152(3):116090. doi:10.1016/j.bone.2021.116090.
53. Kersh ME, Martelli S, Zebaze R, Seeman E, Pandy MG. Mechanical loading of the femoral neck in human locomotion. J Bone Miner Res. 2018;33(11):1999–2006. doi:10.1002/jbmr.3529.
54. Bittner-Frank M, Reisinger AG, Andriotis OG, Pahr DH, Thurner PJ. Cortical and trabecular mechanical properties in the femoral neck vary differently with changes in bone mineral density. JBMR Plus. 2024;8(6):ziae049. doi:10.1093/jbmrpl/ziae049.
55. Holzer G, Von Skrbensky G, Holzer LA, Pichl W. Hip fractures and the contribution of cortical versus trabecular bone to femoral neck strength. J Bone Miner Res. 2009;24(3):468–74. doi:10.1359/jbmr.081108.
56. Scheuren AC, Vallaster P, Kuhn GA, Paul GR, Malhotra A, Kameo Y, et al. Mechano-regulation of trabecular bone adaptation is controlled by the local *in vivo* environment and logarithmically dependent on loading frequency. Front Bioeng Biotechnol. 2020;8:566346. doi:10.3389/fbioe.2020.566346.
57. Walle M, Marques FC, Ohs N, Blauth M, Müller R, Collins CJ. Bone mechanoregulation allows subject-specific load estimation based on time-lapsed micro-CT and HR-pQCT *in vivo*. Front Bioeng Biotechnol. 2021;9:677985. doi:10.3389/fbioe.2021.677985.
58. Subramaniam D, Mat F, Majid MS, Basaruddin KS. Finite element analysis of proximal femur in sideways fall under quasi-static loading. J Mech Sci Technol. 2023;37(7):3315–25. doi:10.1007/s12206-023-2210-y.
59. Grassi L, Schileo E, Taddei F, Zani L, Juszczyk M, Cristofolini L, et al. Accuracy of finite element predictions in sideways load configurations for the proximal human femur. J Biomech. 2012;45(2):394–9. doi:10.1016/j.jbiomech.2011.10.019.
60. Anam C, Triadyaksa P, Naufal A, Arifin Z, Muhlisin Z, Setiawati E, et al. Impact of ROI size on the accuracy of noise measurement in CT on computational and ACR phantoms. J Biomed Phys Eng. 2022;12(4):359–68. doi:10.31661/jbpe.v0i0.2202-1457.

61. Wen XX, Zong CL, Xu C, Ma XY, Wang FQ, Feng YF, et al. Optimal sample volumes of human trabecular bone in μCT analysis within vertebral body and femoral head. Int J Clin Exp Med. 2015;8(10):17868–79. doi:10.1016/j.jmbbm.2016.03.004.
62. Munemoto M, Kido A, Sakamoto Y, Inoue K, Yokoi K, Shinohara Y, et al. Analysis of trabecular bone microstructure in osteoporotic femoral heads in human patients: *in vivo* study using multidetector row computed tomography. BMC Musculoskelet Disord. 2016;17(1):13. doi:10.1186/s12891-015-0848-z.
63. Kim J, Kim JJ. Topology optimization-based localized bone microstructure reconstruction for image resolution enhancement: accuracy and efficiency. Bioengineering. 2022;9(11):644. doi:10.3390/bioengineering9110644.
64. Den Buijs JO, Dragomir-Daescu D. Validated finite element models of the proximal femur using two-dimensional projected geometry and bone density. Comput Methods Programs Biomed. 2011;104(2):168–74. doi:10.1016/j.cmpb.2010.11.008.